7N-34
195449
44P

NASA TN D-51

TECHNICAL NOTE

D-51

THE HYDRODYNAMIC CHARACTERISTICS OF A SUBMERGED LIFTING SURFACE HAVING A SHAPE SUITABLE FOR HYDRO-SKI APPLICATION

By Victor L. Vaughan, Jr.

Langley Research Center
Langley Field, Va.

NATIONAL AERONAUTICS AND SPACE ADMINISTRATION

WASHINGTON October 1959

(NASA-TN-D-51) THE HYDRODYNAMIC CHARACTERISTICS OF A SUBMERGED LIFTING SURFACE HAVING A SHAPE SUITABLE FOR HYDRO-SKI APPLICATION (NASA) 44 p

N89-70465

Unclas
00/34 0195449

1U

NATIONAL AERONAUTICS AND SPACE ADMINISTRATION

TECHNICAL NOTE D-51

THE HYDRODYNAMIC CHARACTERISTICS OF A SUBMERGED LIFTING SURFACE HAVING A SHAPE SUITABLE FOR HYDRO-SKI APPLICATION

By Victor L. Vaughan, Jr.

L
2
0
9

SUMMARY

An experimental investigation was made to determine the hydrodynamic characteristics of an aspect-ratio-0.25 lifting surface having a shape suitable for hydro-ski application and operating at various depths of submersion. Comparisons were made between these data and data previously obtained on a rectangular modified flat plate having an aspect ratio of 0.25 and the same plan-form area. The comparisons indicated that the hydro-ski model had a lower angle of zero lift, a lower lift-curve slope, a lower lift coefficient at the high angles of attack, and a lower lift-drag ratio.

At high angles of attack and high speeds, cavitation at the leading edge caused a large decrease in lift coefficient. At shallow depths of submersion an unstable flow condition was encountered during cavitation because of small amounts of air bleeding intermittently into the cavitated region through the trailing vortices and then being dissipated by entrainment in the water; thus a fluctuating pressure in the cavity on the upper surface of the model resulted.

Two types of ventilation, the partial bubble and the full bubble, were encountered at shallow depths of submersion and high speeds. This ventilation corresponds to that encountered in previous investigations of flat plates. However, both types of bubble caused sharp decreases in the lift, drag, and pitching moment while the previous flat-plate data showed that only the full bubble caused sharp decreases in the forces and moments. The cavitation and ventilation boundaries moved to higher speeds for a given angle of attack for the hydro-ski model than they did for the flat-plate model.

INTRODUCTION

The interest shown in obtaining information on the hydrodynamic characteristics of lifting surfaces operating beneath the free water surface resulted in a series of investigations being conducted by the National Aeronautics and Space Administration on low-aspect-ratio rectangular modified flat plates operating at various depths of submersion. The results of these investigations are reported in references 1 to 4. Since their scope was limited to flat plates, the present investigation was undertaken to obtain comparable information on a low-aspect-ratio lifting surface that has been shown to be a practical shape for an actual hydro-ski. A ski similar to this shape has been tested on both a 1/8-size dynamic model (ref. 5) and a full-scale Grumman JRF-5 airplane and was found to be suitable for operation on water, snow, and ice. The present paper presents data obtained in Langley tank no. 2 at various depths of submersion. The flow characteristics observed and their effects are discussed in some detail.

L
2
0
9

APPARATUS AND PROCEDURE

Description of Model

The lines of the model and a table of offsets are shown in figure 1. The plan-form area (50 sq in.) and the aspect ratio of the model were the same as the aspect-ratio-0.25 flat plates reported in references 1 to 4. The form included a rounded leading edge, a tapered trailing edge, upper surface camber, and a planing bottom which was laterally concave near the chines and convex at the keel. The maximum thickness was 10.55 percent of the model length and occurred at 30 percent of the length. The model was made of plastic which was polished to a smooth finish and had a steel inner core.

The strut (also shown in fig. 1) had an NACA 66_1-012 airfoil section and was the same as that used in reference 2. It was mounted so that its leading edge was 8.94 inches forward of the hydro-ski trailing edge, perpendicular to the keel, and intersected the upper surface of the model without fillets. The strut was made of stainless steel and was polished to a smooth finish.

Test Methods and Equipment

The tests were made by using the Langley tank towing carriage with electrical strain-gage balances to measure the lift, drag, and pitching

moment. The pitching moment was measured about an arbitrary point above the model and converted to the pitching moment about the trailing edge.

A wind screen was used to reduce the aerodynamic tares to negligible values. The hydrodynamic strut tares were not subtracted from the data. Force measurements were made at constant speeds for fixed angles of attack and depths of submersion. The angle of attack is defined as the angle measured between the straight portion of the keel and the water surface. Depth of submersion is defined as the distance from the undisturbed water surface to the center of the leading edge of the model. (See fig. 1.)
L Tests were made at depths of submersion of 1.0, 1.5, 3.0, and 6.0 inches
2 over a range of angles of attack from -2° to 20° and at speeds up to
0 approximately 85 feet per second. The speeds and angles of attack at
9 which ventilation occurred were also determined at a depth of submersion of 0.5 inch. Figure 2 shows the test setup with the model and wind screen in place.

The changes in angle of attack and the accompanying changes in depth of submersion due to the structural deflections were measured during the calibration of the balances and were found to be negligible for the combinations of forces encountered. The estimated accuracy of the measurements is as follows:

Angle of attack, deg	±0.1
Depth of submersion, in.	±0.1
Speed, fps	±0.2
Lift, lb	±5.0
Drag, lb	±5.0
Pitching moment, ft-lb	±1.8

The forces and moments were converted to the usual aerodynamic coefficient form by using a measured value of the density of water of 1.942 slugs/cu ft and a constant plan-form area of 0.347 square foot. The kinematic viscosity measured during the tests was 1.67×10^{-5} sq ft/sec.

RESULTS AND DISCUSSION

A short motion-picture film supplement illustrating the cavitating and ventilating flow characteristics discussed in this paper is available on loan. A request card form and a description of the film will be found at the end of this paper.

Force and Moment Data

The basic experimental data are presented in figures 3 to 5 as plots of lift, drag, and pitching moment about the trailing edge as a function of speed with angle of attack as the parameter. Data are presented for the four depths of submersion investigated. The scatter and discontinuities at the high angles of attack and high speeds are due to cavitation and ventilation and will be discussed subsequently.

General Characteristics

L
2
0
9

The lift coefficients C_L for the four depths of submersion investigated are presented in figure 6 as a function of angle of attack with speed as the parameter. This figure shows that, for angles of attack below 9°, the lift coefficient did not vary with speed above a speed of 20 feet per second. At a speed of 20 feet per second, the lift coefficient was lower than at the higher speeds. As the depth of submersion decreased, the lift coefficient at 20 feet per second approached the value of lift coefficient at the higher speeds.

Figure 6(a) shows that the angle of zero lift at a depth of submersion of 1.0 inch is -2°. Extrapolation of the curves of figure 6 indicated the angle of zero lift decreased as the depth of submersion increased.

The lift-drag ratio curves of figure 7 show that at noncavitating and nonventilating speeds the maximum lift-drag ratio occurred between angles of attack of 7° and 8° depending on the depth of submersion. The effects of depth of submersion are small but, generally at angles of attack lower than that for maximum lift-drag ratio, the lift-drag ratio increased with increasing depth of submersion. As the angle of attack approached 20°, the lift-drag ratio decreased with a diminishing effect of depth of submersion.

Flow Changes and Effects

Cavitation.- The angles of attack at which cavitation at the rounded leading edge was visually observed are shown by the vertical arrows for each speed in figure 6. Cavitation did not develop at any speed below 40 feet per second for the angles of attack investigated. At high angles of attack an increase in lift coefficient was noted with increasing speed followed by a decrease with increasing extent of cavitation. This effect may be seen better in figure 8 which is a plot of lift coefficient C_L, drag coefficient C_D, and pitching-moment coefficient about the trailing edge C_m against speed. The force and moment coefficient curves are

very similar in character. The decrease in drag coefficient at speeds above 60 feet per second was evidently caused by a drop in the induced drag coefficient as a result of the large decrease in lift coefficient in this speed range. The vertical dashed line in figure 8 indicates the speed at which cavitation was first observed.

An unstable condition occurred during cavitation at the shallow depths of submersion and is shown by the hatched area in figure 8(b) for a depth of submersion of 1.5 inches. The instability was evidently caused by small amounts of air bleeding intermittently into the cavitated region through the trailing vortices and then being dissipated by entrainment in the water; thus fluctuating pressure in the cavity on the upper surface of the model resulted.

L
2
0
9

Sequence photographs of a typical run showing cavitation at an angle of attack of 20° and a depth of submersion of 1.5 inches are presented in figure 9. At a speed of 44.3 feet per second the cavitation has just become visible and has spread across the leading edge of the model. The streamers attached to the leading edge and fading out about three chord lengths behind the model are the cavitated cores of the trailing vortices. There is apparently no air entrained in the vortices at this speed. At speeds of 64.3 and 68.9 feet per second, the cavitation has increased until it covers the upper surface of the model back to the strut. The characteristic white appearance of the cavitation can be seen in the photographs, the cavitated vortices showing their characteristic helical form. At a speed of 74.2 feet per second a change in the appearance of the cavitation may be noted. The white appearance has cleared up slightly and the cavitated region looks more like a bubble. The increased disturbance in the trailing vortices, as indicated by the arrows, shows entrainment of air has occurred. At speeds of 79.0 and 83.9 feet per second the previously noted white appearance of cavitation at the leading edge is completely gone, the cavitated area is clear, and separation of the water from the upper surface of the model is shown. At 79.0 feet per second the location of disturbance due to entrainment of air in the vortices is about the same as it was at 74.2 feet per second. However, at 83.9 feet per second the disturbance has moved forward to the trailing edge of the model.

Cavitation followed by ventilation.- The lift-coefficient plot (fig. 6) at a depth of submersion of 1.0 inch shows the effects of both cavitation and ventilation. Ventilation is due to atmospheric air entering the low-pressure regions which results in varying degrees of increased pressure in these regions. The hatched area is the unstable cavitation region (observed at both 60 and 80 feet per second) and is the same as previously explained. The sharp drop in lift coefficient at 60 and 80 feet per second is caused by ventilation of the model.

At a depth of submersion of 1.0 inch, cavitation was visually observed at 40 feet per second for all angles of attack above 4°; therefore, ventilation was preceded by cavitation. Two types of ventilation were noted, the partial bubble which is associated with high angles of attack and the full bubble which is associated with the lower angles of attack. (See refs. 1, 2, and 4.)

The force and moment coefficients at an angle of attack of 20° and a depth of submersion of 1.0 inch are presented in figure 10. The vertical dashed line indicates the speed at which cavitation was first observed. Previous investigations on flat plates had indicated very little change in the force and moment coefficients with the formation of the partial bubble. However, with the present model, as can be seen in figure 10 at a speed of 54 feet per second, the force and moment coefficients decreased sharply to approximately 50 percent of their original value with the formation of the partial bubble, and showed extensive pressure relief on the upper surface of the model. After the partial bubble formed, the force and moment coefficients remained constant with increasing speed.

The sequence photographs of a typical run showing cavitation, transition from cavitation to ventilation, and ventilation (partial bubble) are presented in figure 11 for an angle of attack of 20° and a depth of submersion of 1.0 inch. The arrows indicate the disturbed region in the trailing vortices caused by the entrainment of air. At 44.8 feet per second the model is cavitated as shown by the white appearance across the leading edge. Transition from cavitation to ventilation occurred at 54 feet per second as shown by the photographs at this speed. The first of the two photographs at 54 feet per second shows cavitation whereas the second photograph shows what happens during transition from cavitation to ventilation. At the completion of transition and while the speed is still 54 feet per second, the ventilation bubble collapsed so that it looked similar to the photograph at 59.6 feet per second. This is the partial-bubble type of ventilation at which the cavity pressure is somewhat less than atmospheric and yet somewhat greater than vapor pressure such as in a cavitation bubble. At 64.0 and 68.8 feet per second, the partial bubble has grown so that the point of flow reattachment has moved back near the trailing edge of the model.

At low angles of attack (below 18°) at a depth of submersion of 1.0 inch and before ventilation occurred, the unstable condition during cavitation, noted previously, increased in intensity until a severe lateral and vertical oscillation of the model and supporting gear developed. This unstable condition is shown by the hatched area in figure 12 for an angle of attack of 14°. The oscillation increased in intensity until ventilation occurred. The ventilation took the form of the full bubble and caused a sharp drop in the force and moment coefficients comparable to that of the partial bubble. When ventilation occurred, the oscillation, cavitation, and vortices were all eliminated; afterwards,

the force and moment coefficients remained at a constant value with increasing speed.

The sequence photographs of a typical run showing cavitation, oscillation, and ventilation (full bubble) are presented in figure 13 for an angle of attack of 14° and a depth of submersion of 1.0 inch. The arrows indicate the disturbed region in the trailing vortices caused by the entrainment of air. The photographs at 44.5, 54.0, and 59.4 feet per second show increasing extent of cavitation as the speed is increased. The unstable condition during cavitation, noted previously, has already started at 59.4 feet per second as may be seen in figure 12 at that speed. As this instability increased in intensity, it caused vertical and horizontal oscillation of the model and supporting gear which is indicated by the blurred appearance in the photographs at 64.4 and 69.8 feet per second. (See fig. 13.) This oscillation increased in intensity until the model ventilated and a full bubble formed. The last photograph at 74.4 feet per second shows the full-bubble type of ventilation at which the cavity pressure is atmospheric.

L
2
0
9

Comparison With Previous Experiments

The lift and drag characteristics of the present 10.55-percent-thick hydro-ski model are compared in figure 14 with those of the 2.65-percent-thick aspect-ratio-0.25 flat-plate model of reference 2. The results shown are for a depth of submersion of 6.0 inches and at speeds of 10, 50, and 80 feet per second to cover the conditions of no cavitation, cavitation, and severe cavitation, respectively. In general, the lift-coefficient curves show that the angle of zero lift, lift-curve slope, and lift coefficient at the high angles of attack are lower for the hydro-ski model than for the flat-plate model.

The results of the investigation on the flat plate (ref. 2) had shown that the lift coefficient did not vary with speed for angles of attack below 12° and speeds below 50 feet per second except at the very low speeds where the lift coefficient was lower. This was essentially true for the hydro-ski model for angles of attack below 9°. The effects of cavitation were a little more pronounced for the hydro-ski model than for the flat-plate model at high speed. The lift-drag polar shows that the two models give curves similar in character but with the drag coefficient higher for a given lift coefficient for the hydro-ski model.

Figure 15 is a plot of the maximum lift-drag ratio against depth of submersion. The maximum lift-drag ratio increased slightly with increasing depth of submersion for the hydro-ski model and decreased slightly with increasing depth of submersion for the flat-plate model.

The cavitation boundaries as visually observed during the testing of the hydro-ski model are compared with the cavitation boundaries of the flat plate (ref. 2) in figure 16. The curves represent the first speed for a given angle of attack at which cavitation was visually observed. For the flat-plate model, cavitation occurred at approximately the same speed for all depths of submersion and the curve shows that the speed at which cavitation started decreased as the angle of attack increased up to 12° and remained at a constant value of 30 feet per second for higher angles of attack. For the hydro-ski model, the inception of cavitation was at approximately 40 feet per second for all angles of attack above 4° at a depth of submersion of 1.0 inch. At depths of submersion of 6.0, 3.0, and 1.5 inches, the speed at which cavitation started decreased rapidly to 40 feet per second as the angle of attack increased to 12° and thereafter remained at 40 feet per second for higher angles of attack. It may be noted in figure 16 that the speed at which cavitation was first visually observed did not change with increasing angle of attack above 12° for either model.

The ventilation boundaries for the two models, as defined by the appearance of the bubble that caused sharp decreases in the forces and moments, are presented in figure 17 for depths of submersion of 0.5 and 1.0 inches. The ventilation boundaries are at higher speeds for a given angle of attack for the hydro-ski model than for the flat-plate model.

CONCLUSIONS

The results of the investigation indicated the following:

1. The hydro-ski model had a lower angle of zero lift, lift-curve slope, lift coefficient at the high angles of attack, and lift-drag ratio than the flat-plate model reported in NACA Technical Note 3908.

2. At high angles of attack and high speeds, cavitation became severe and caused a large decrease in lift coefficient. At shallow depths of submersion an unstable flow condition developed during this cavitation because of intermittent ventilation of the cavity.

3. Two types of ventilation, the partial bubble and the full bubble, were encountered at the shallow depths of submersion and high speeds. Both types of bubble caused a sharp decrease in the lift, drag, and pitching moment for the hydro-ski model while only the full bubble caused a sharp decrease in the forces and moments for the flat-plate model.

4. The cavitation and ventilation boundaries moved to higher speeds for a given angle of attack for the hydro-ski model than for the flat-plate model.

Langley Research Center,
National Aeronautics and Space Administration,
Langley Field, Va., June 30, 1959.

L
2
0
9

REFERENCES

1. Wadlin, Kenneth L., Ramsen, John A., and Vaughan, Victor L., Jr.: The Hydrodynamic Characteristics of Modified Rectangular Flat Plates Having Aspect Ratios of 1.00, 0.25, and 0.125 and Operating Near a Free Water Surface. NACA Rep. 1246, 1955. (Supersedes NACA TN's 3079 by Wadlin, Ramsen, and Vaughan and 3249 by Ramsen and Vaughan.)

2. Vaughan, Victor L., Jr., and Ramsen, John A.: Hydrodynamic Characteristics Over a Range of Speeds Up to 80 Feet Per Second of a Rectangular Modified Flat Plate Having an Aspect Ratio of 0.25 and Operating at Several Depths of Submersion. NACA TN 3908, 1957.

3. Ramsen, John A., and Vaughan, Victor L., Jr.: Hydrodynamic Tares and Interference Effects for a 12-Percent-Thick Surface-Piercing Strut and an Aspect-Ratio-0.25 Lifting Surface. NACA TN 3420, 1955.

4. Ramsen, John A.: An Experimental Hydrodynamic Investigation of the Inception of Vortex Ventilation. NACA TN 3903, 1957.

5. Wadlin, Kenneth L., and Ramsen, John A.: Tank Investigation of the Grumman JRF-5 Airplane Fitted With Hydro-Skis Suitable for Operation on Water, Snow, and Ice. NACA RM L9K29, 1950.

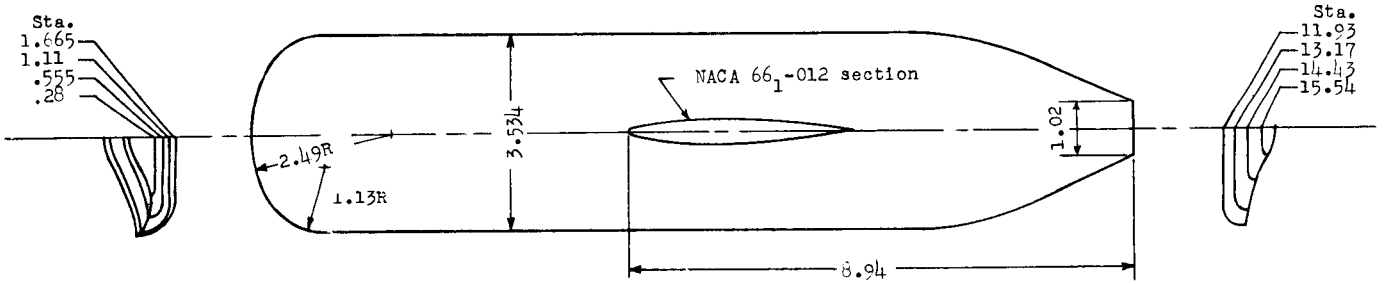

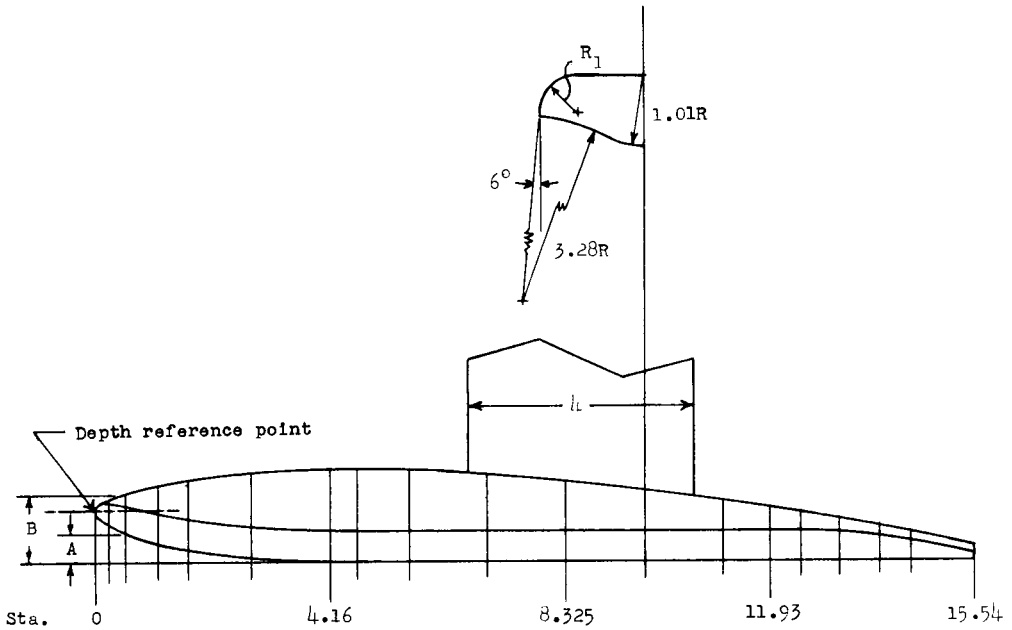

TABLE OF OFFSETS			
Sta.	R_1	A	B
.000	-	.880	.880
.280	.079	.650	1.100
.555	.220	.500	1.190
1.110	.505	.310	1.330
1.665	.630	.180	1.430
2.775		.050	1.570
4.160		.003	1.640
4.660		.000	-
5.550			1.630
6.940			1.550
8.325			1.430
9.710	.630		1.280
11.100	.440		1.085
11.930	.310		-
12.490	.220		.870
13.170	.220		-
13.875	.170		.610
14.430	.130		-
15.540	.130	.000	.250

Figure 1.- Details of model. Dimensions are in inches.

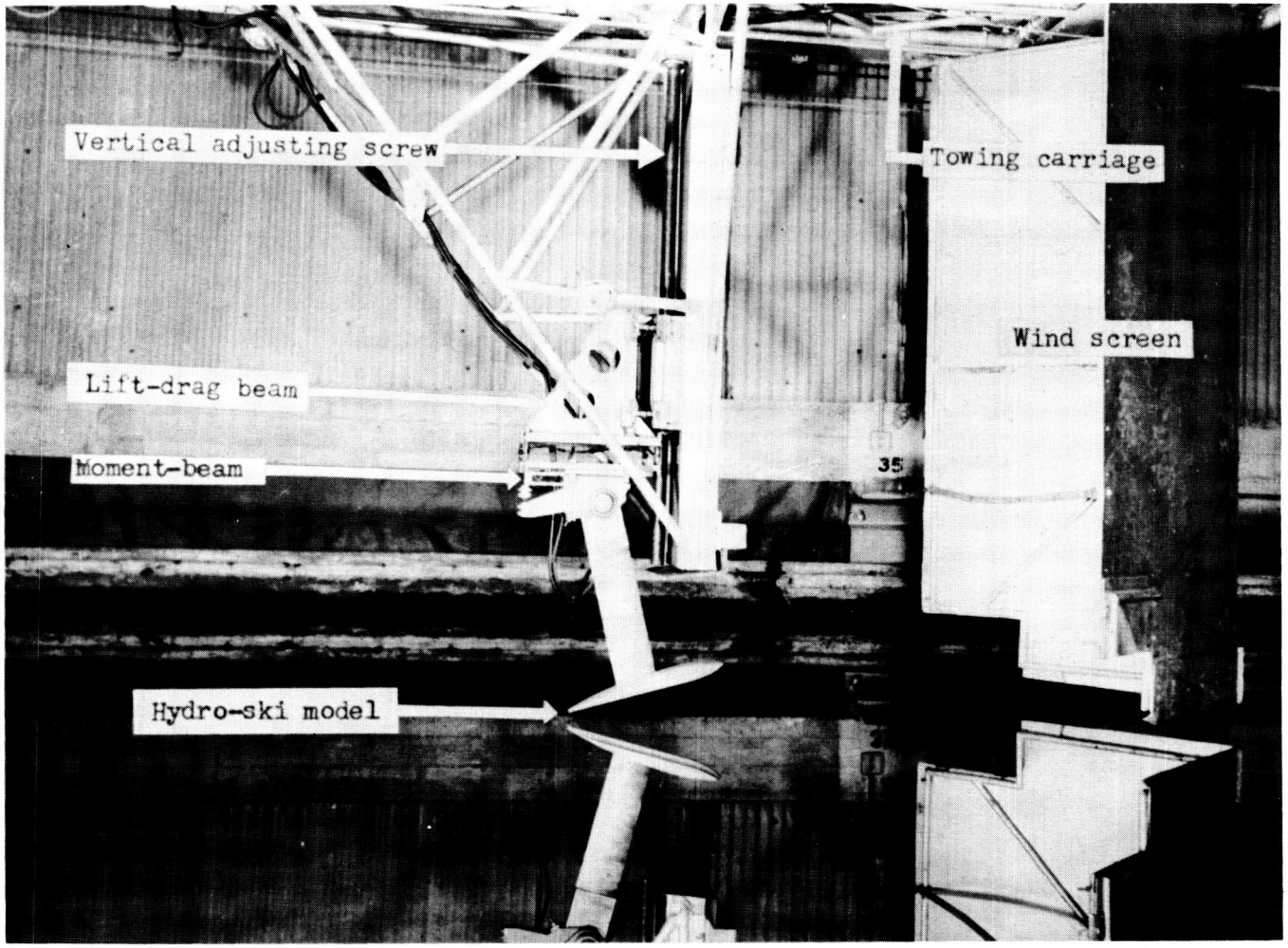

Figure 2.- Photograph of test setup with wind screen in place. L-59-3079

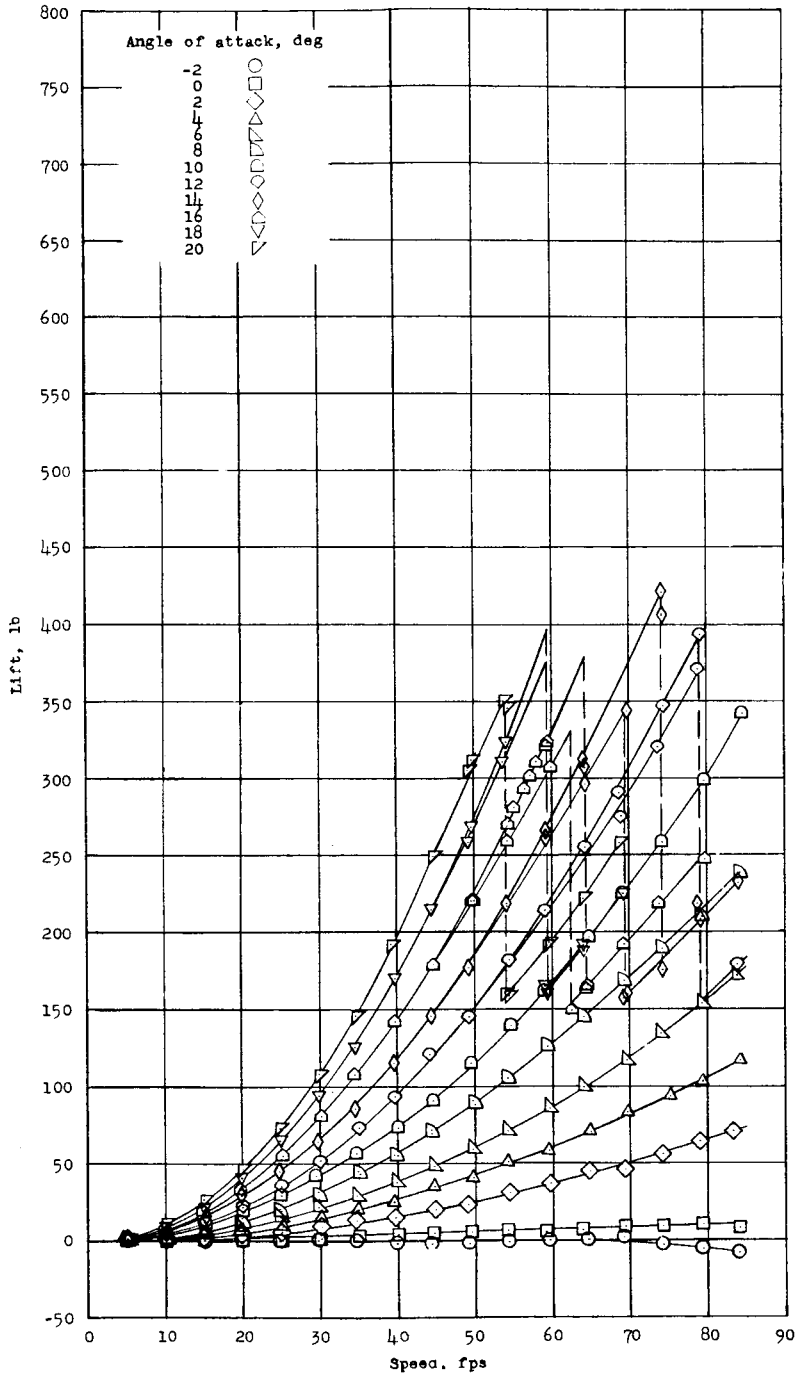

(a) Depth of submersion, 1.0 inch.

Figure 3.- Lift on the hydro-ski model.

L-209

L-209

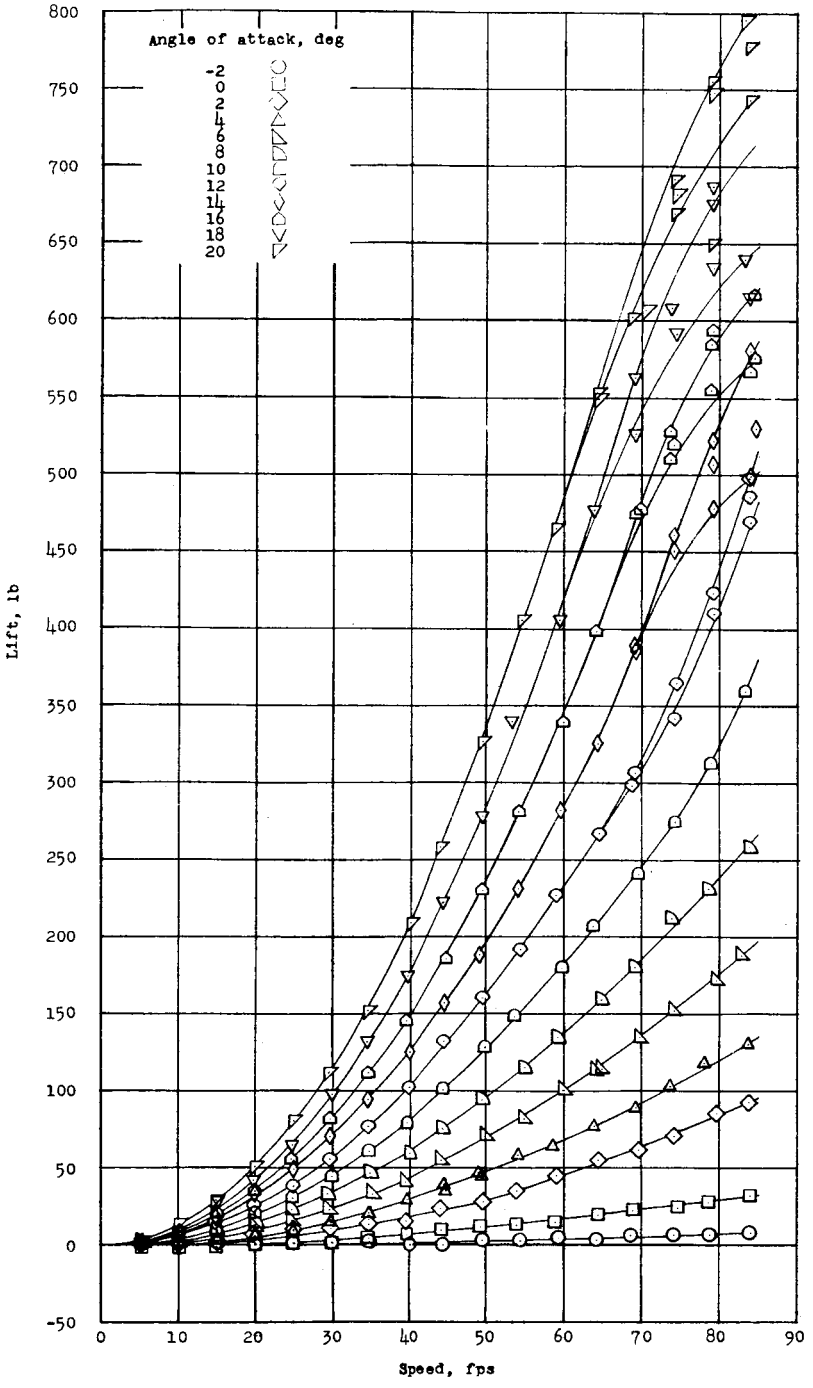

(b) Depth of submersion, 1.5 inches.

Figure 3.- Continued.

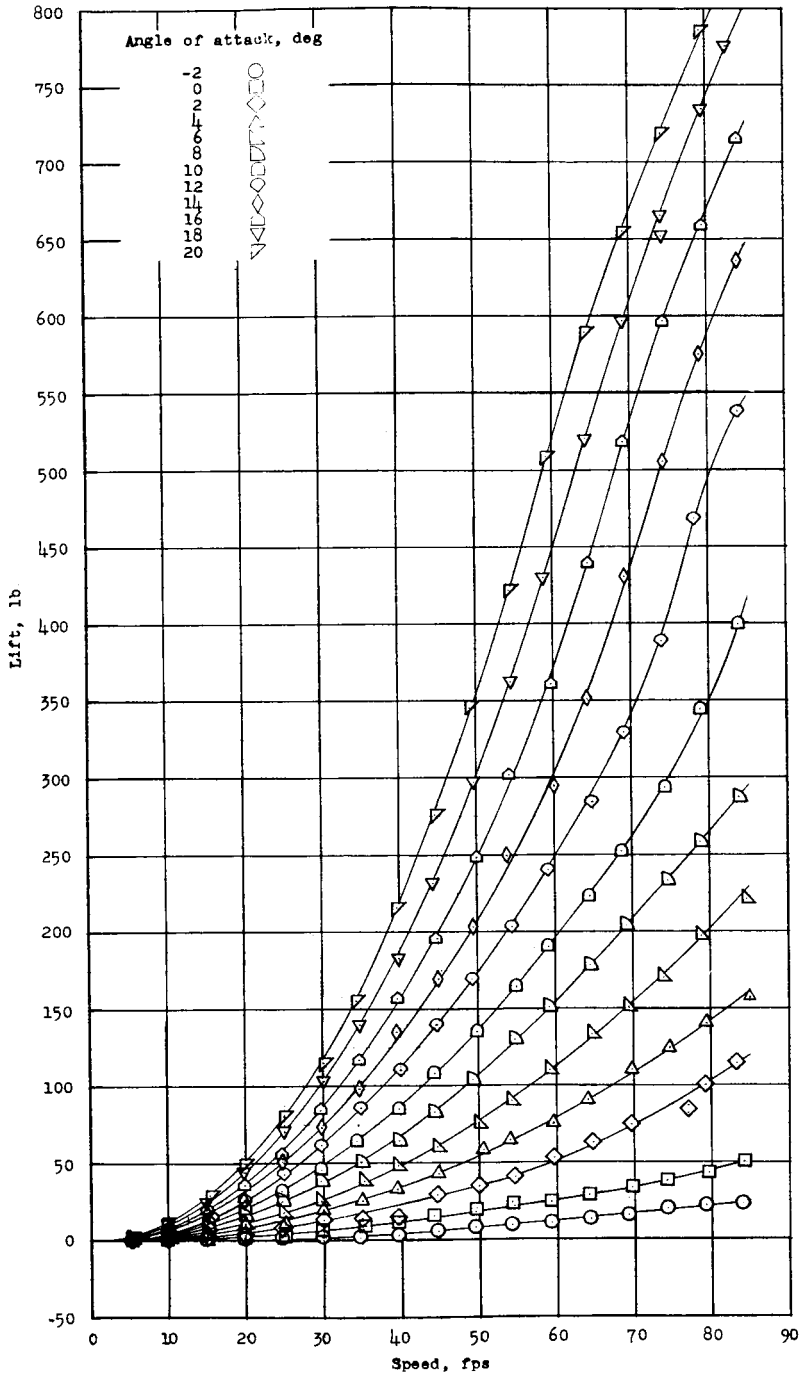

(c) Depth of submersion, 3.0 inches.

Figure 3.- Continued.

L-209

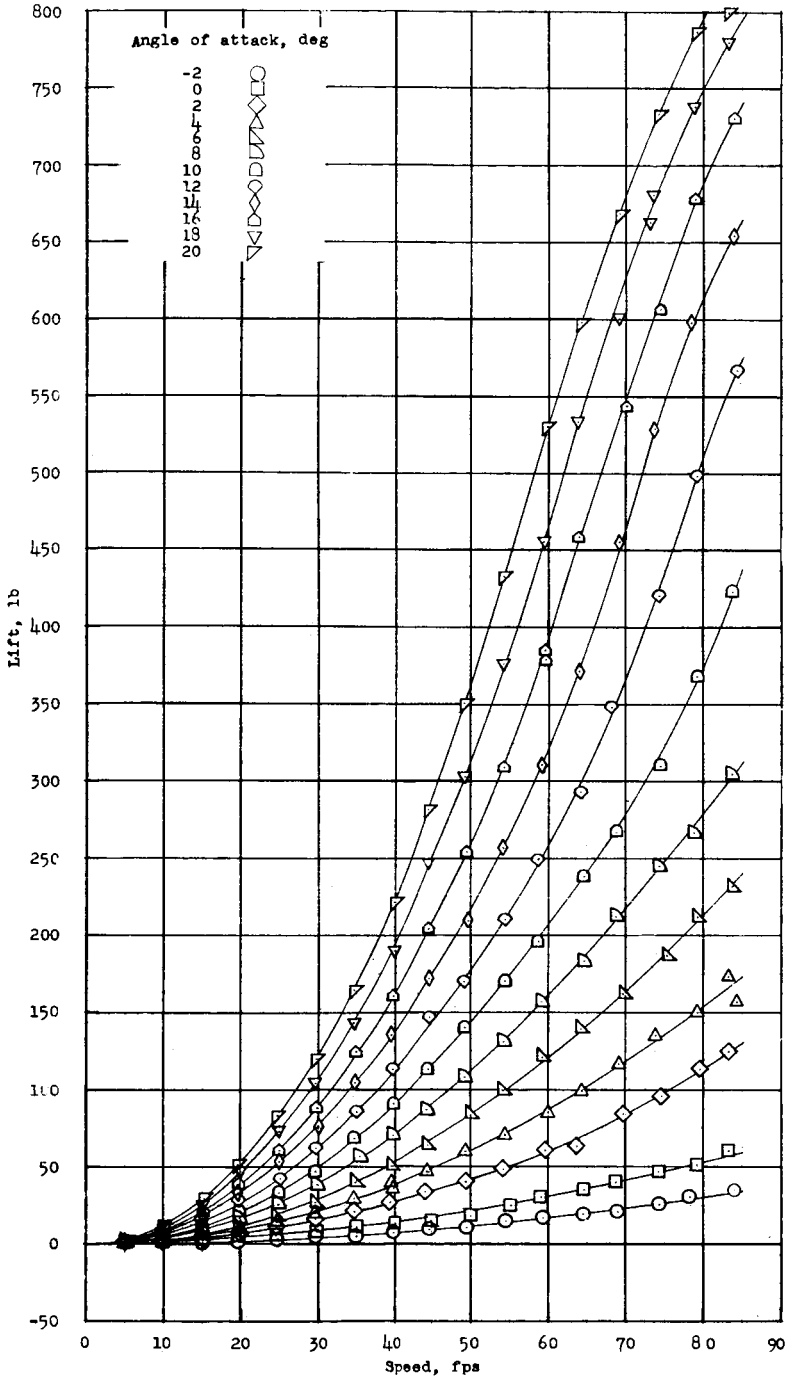

(d) Depth of submersion, 6.0 inches.

Figure 3.- Concluded.

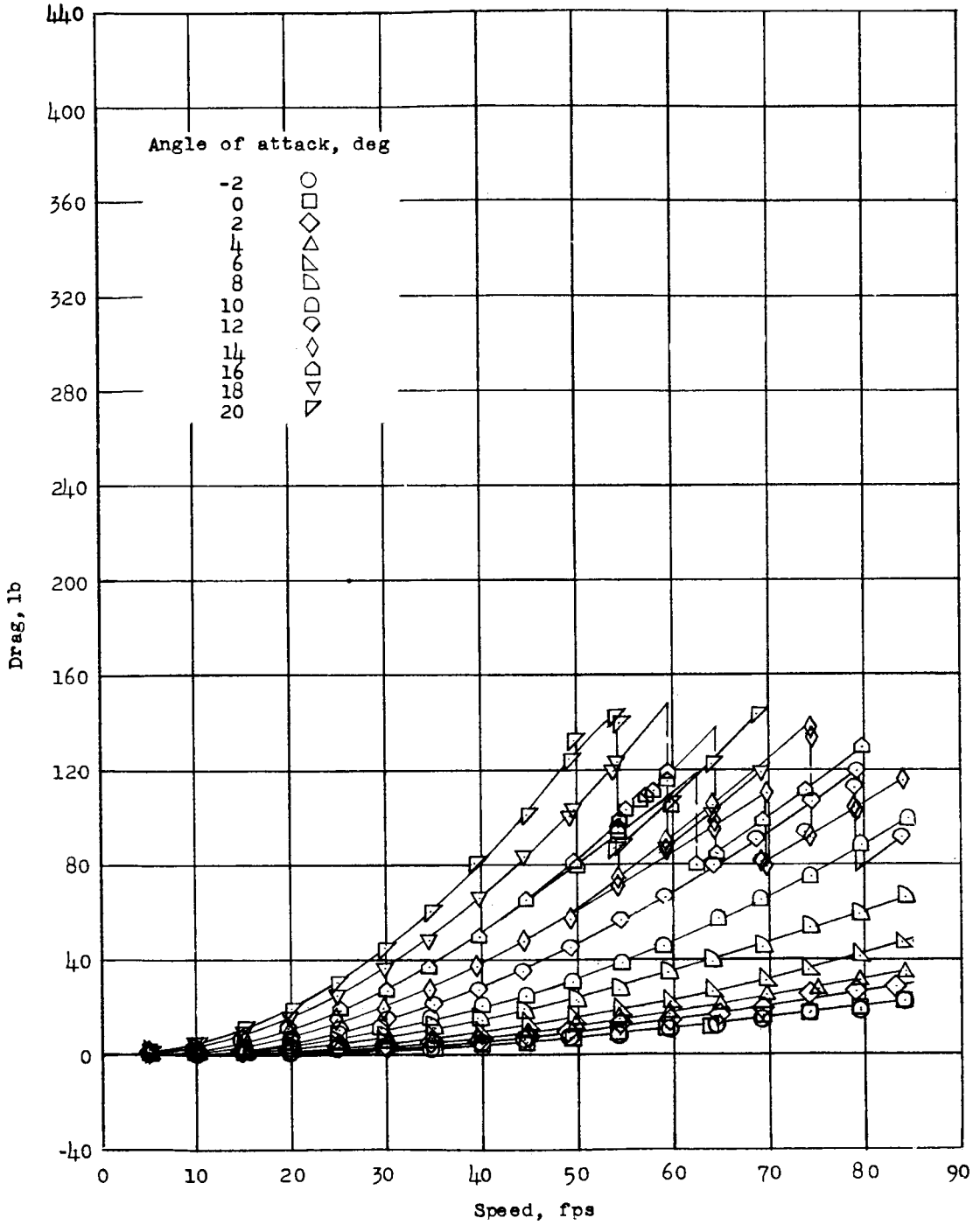

(a) Depth of submersion, 1.0 inch.

Figure 4.- Drag on the hydro-ski model.

L-209

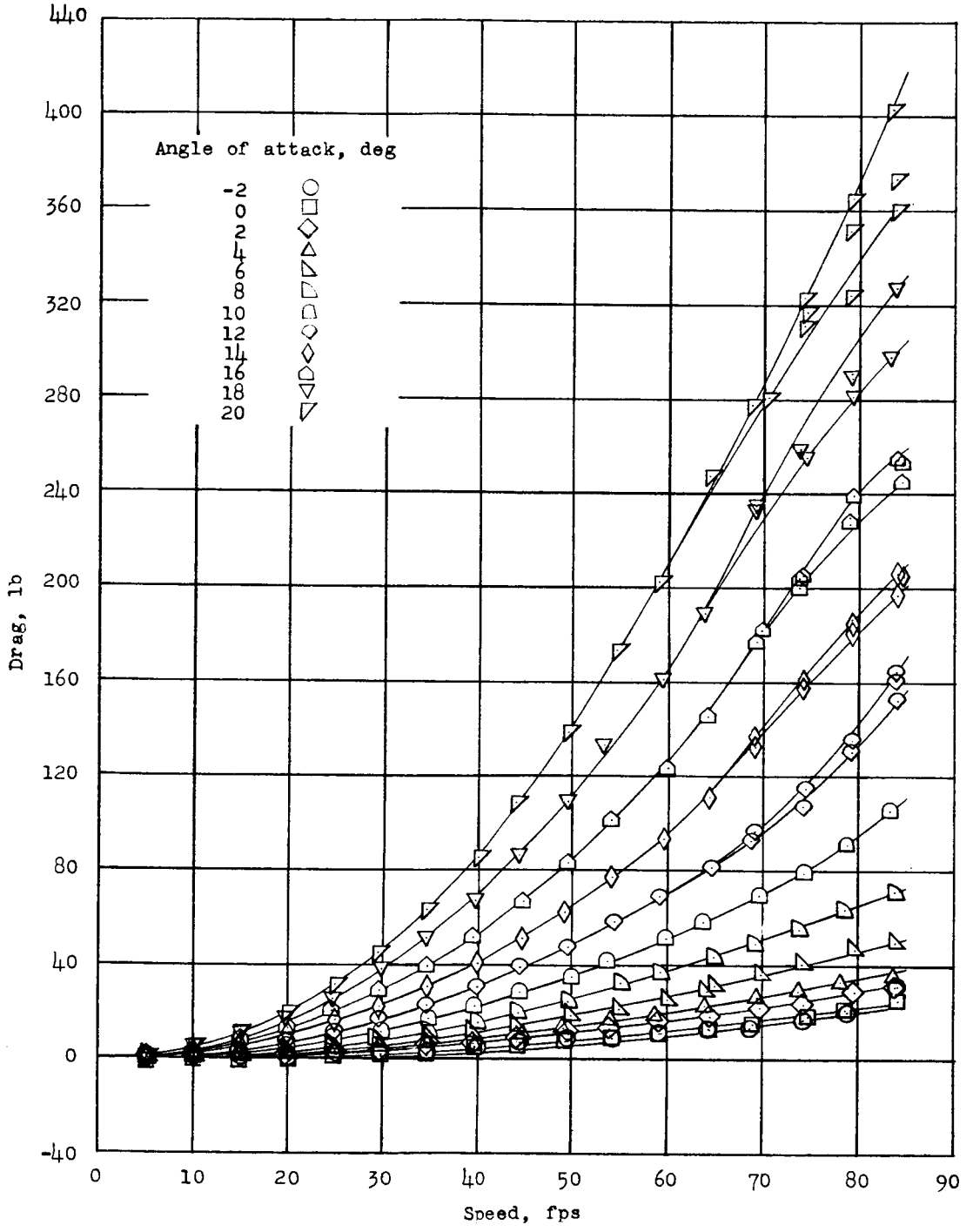

(b) Depth of submersion, 1.5 inches.

Figure 4.- Continued.

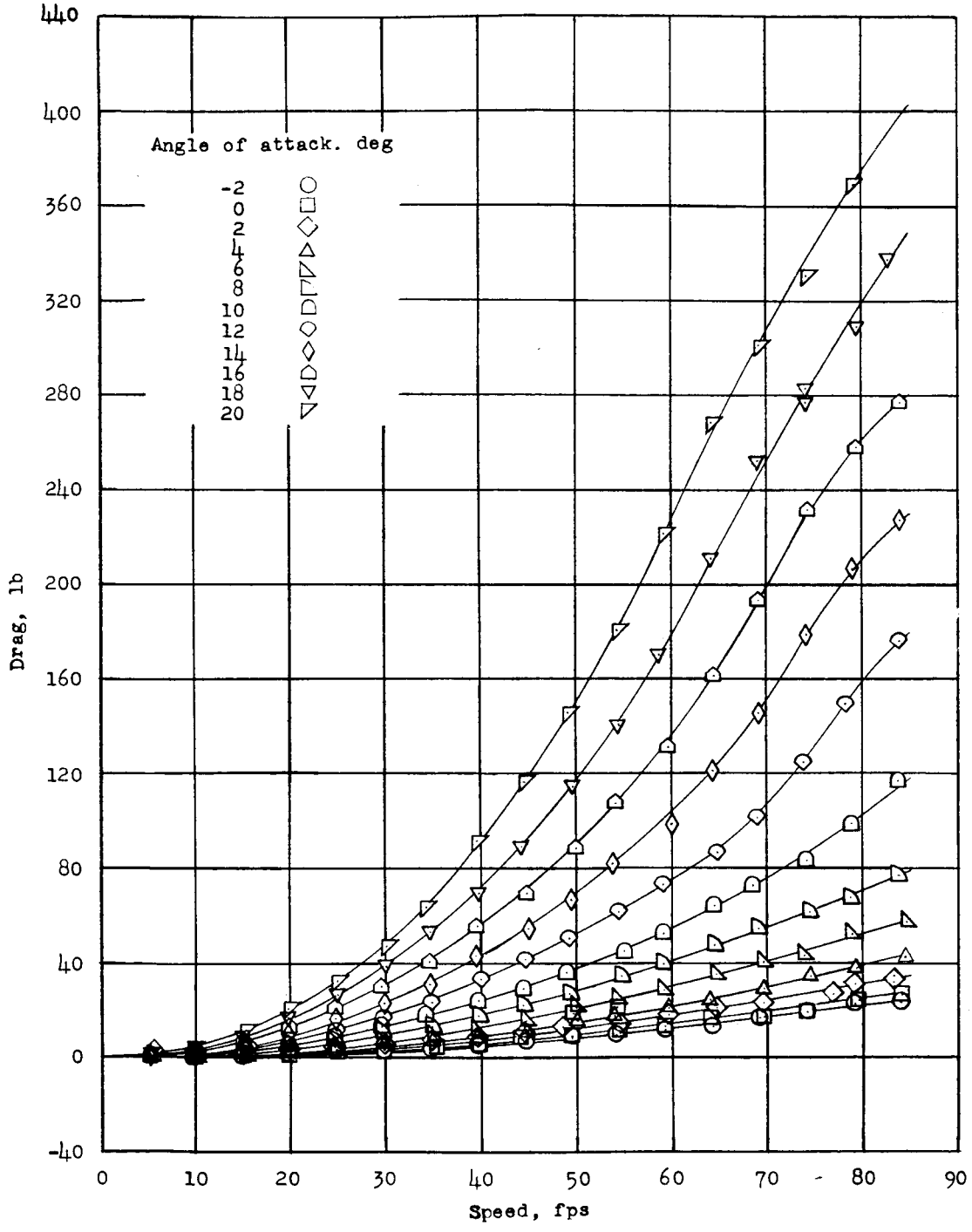

(c) Depth of submersion, 3.0 inches.

Figure 4.- Continued.

L-209

L-209

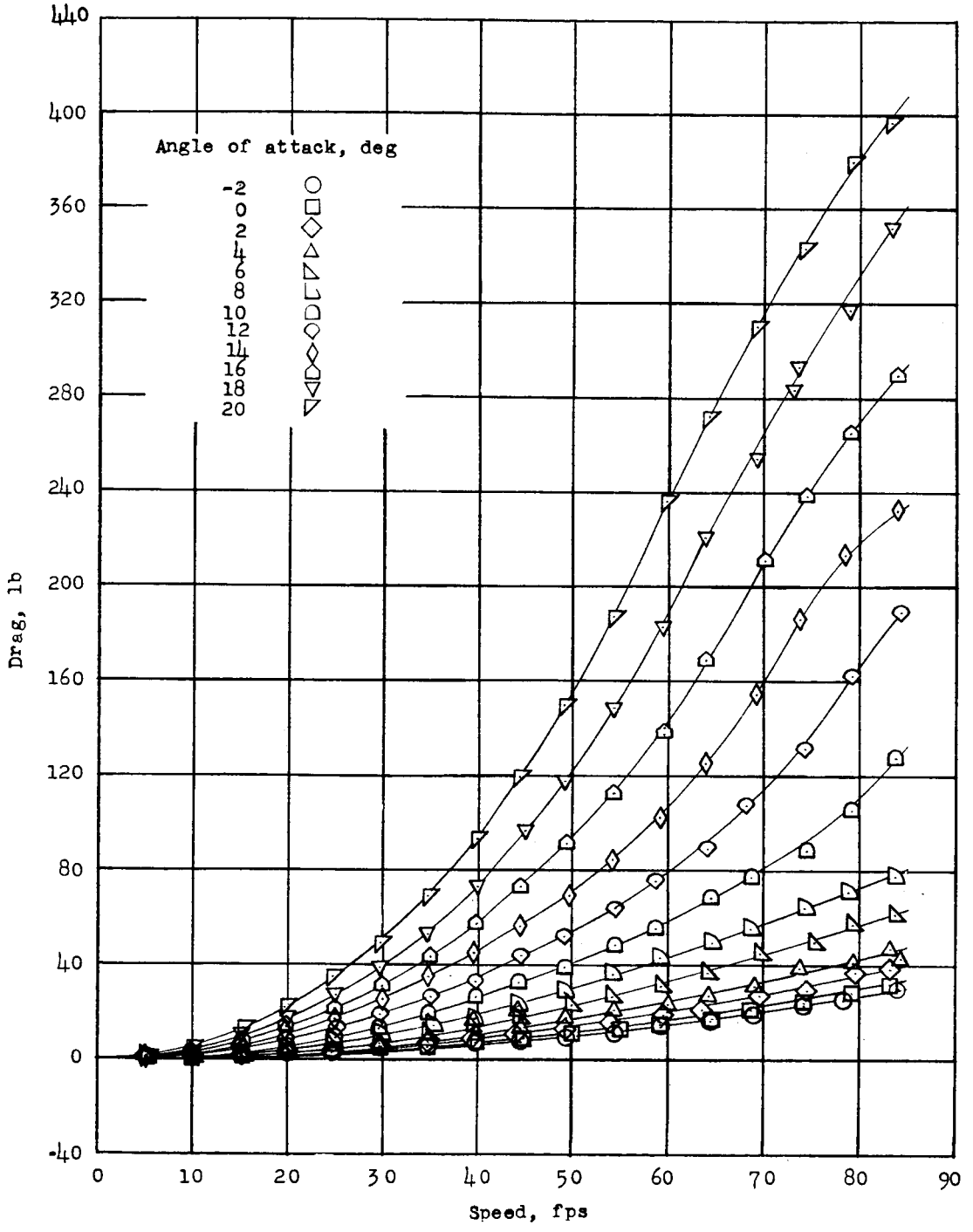

(d) Depth of submersion, 6.0 inches.

Figure 4.- Concluded.

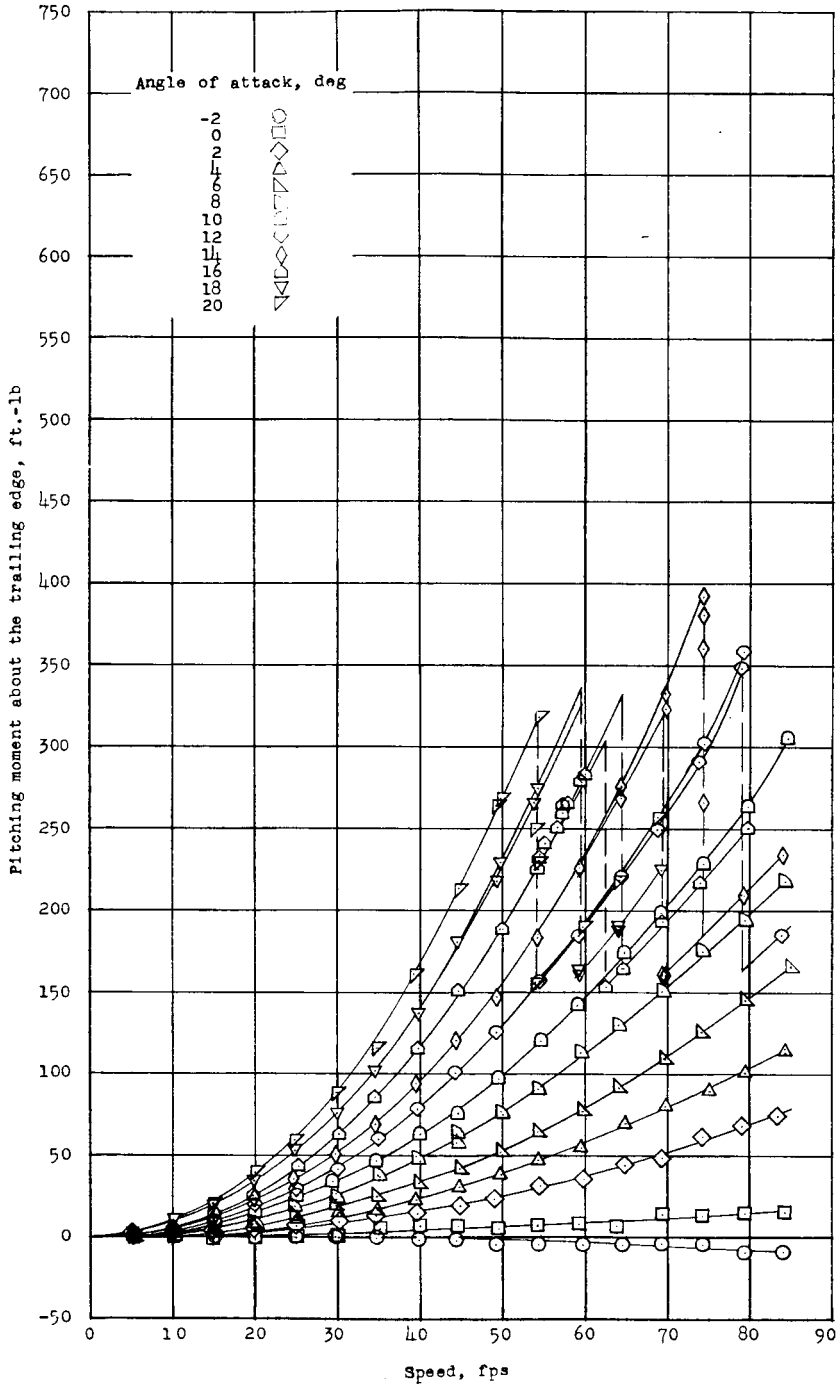

(a) Depth of submersion, 1.0 inch.

Figure 5.- Pitching moment on the hydro-ski model.

L-209

L-209

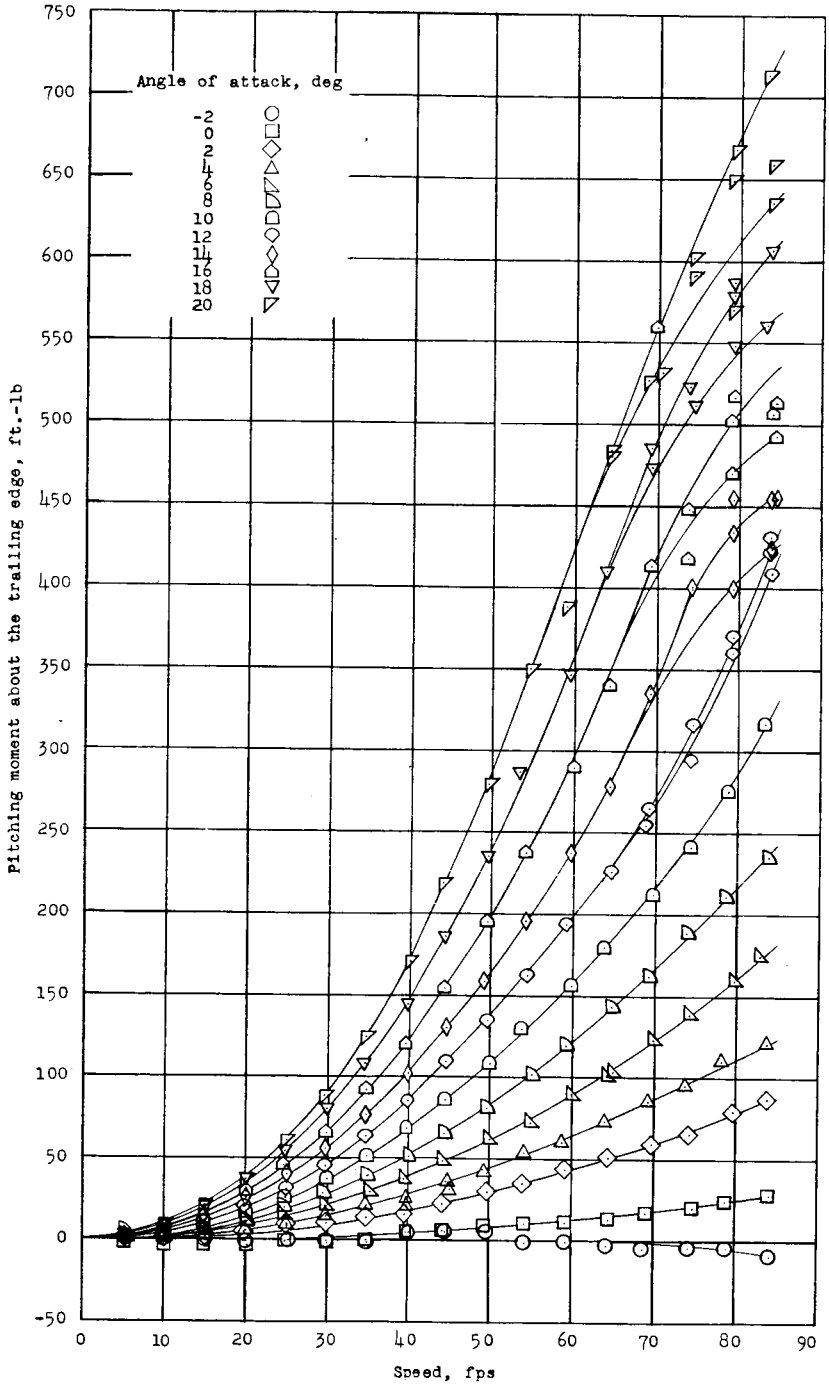

(b) Depth of submersion, 1.5 inches.

Figure 5.- Continued.

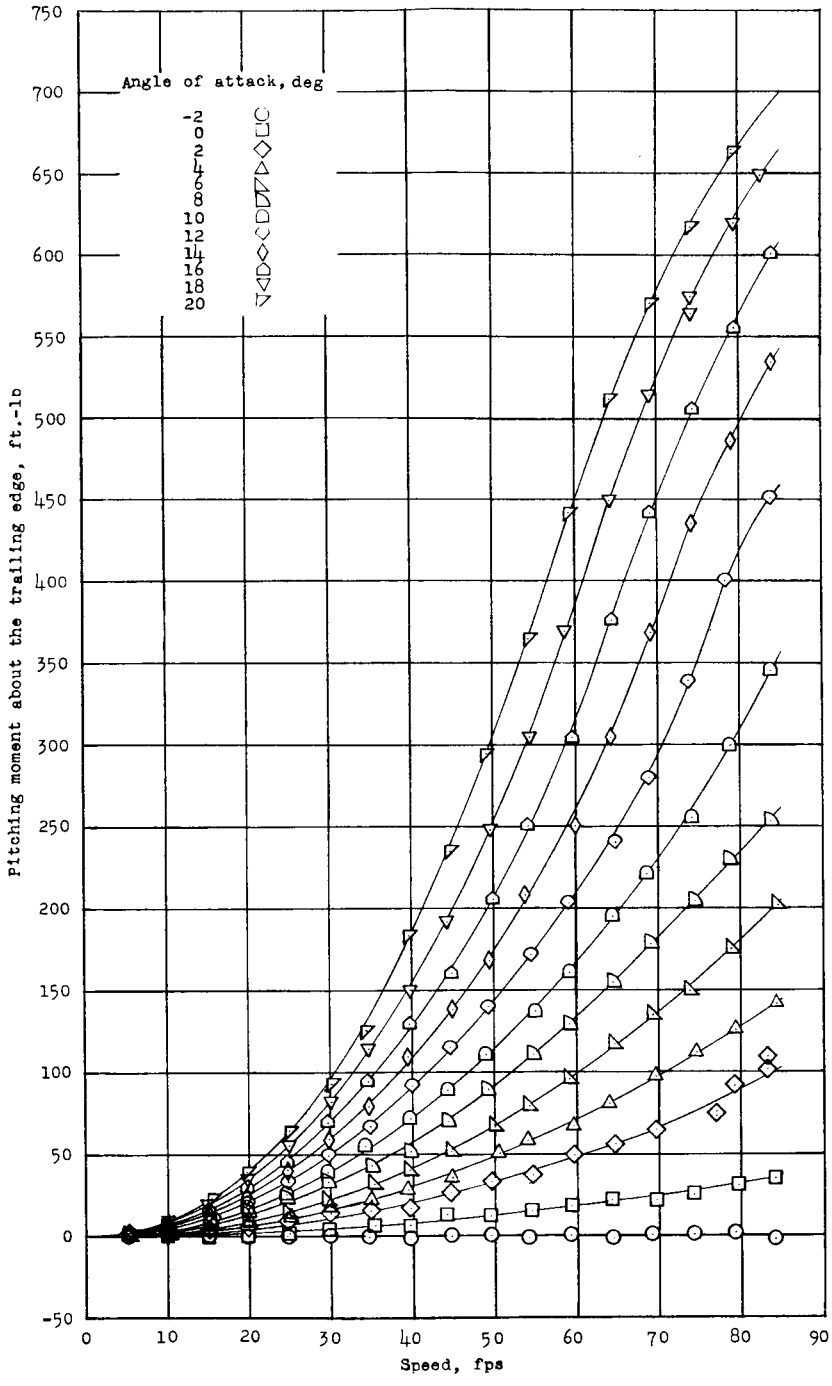

(c) Depth of submersion, 3.0 inches.

Figure 5.- Continued.

L-209

L-209

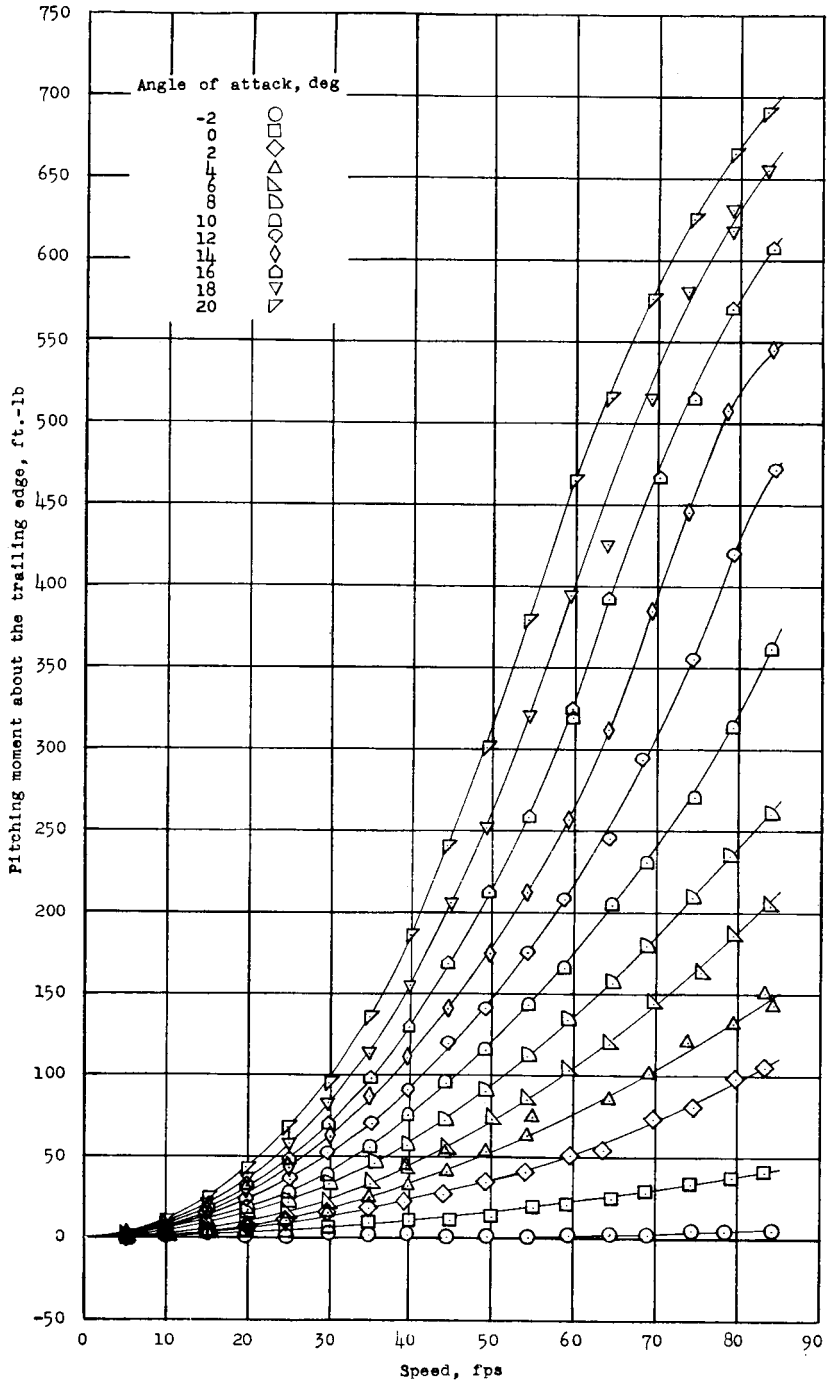

(d) Depth of submersion, 6.0 inches.

Figure 5.- Concluded.

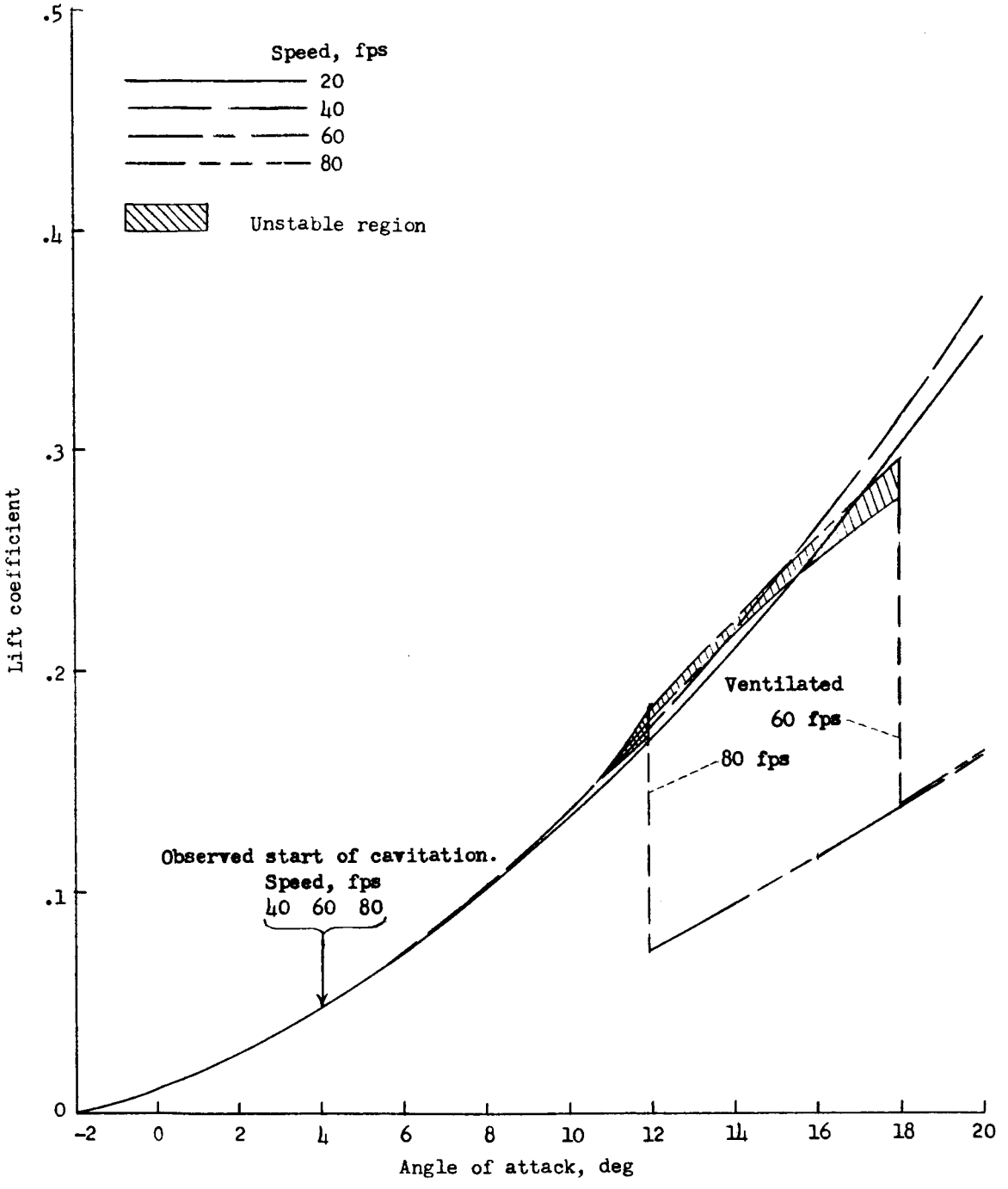

(a) Depth of submersion, 1.0 inch.

Figure 6.- Lift coefficients at various depths of submergence.

L-209

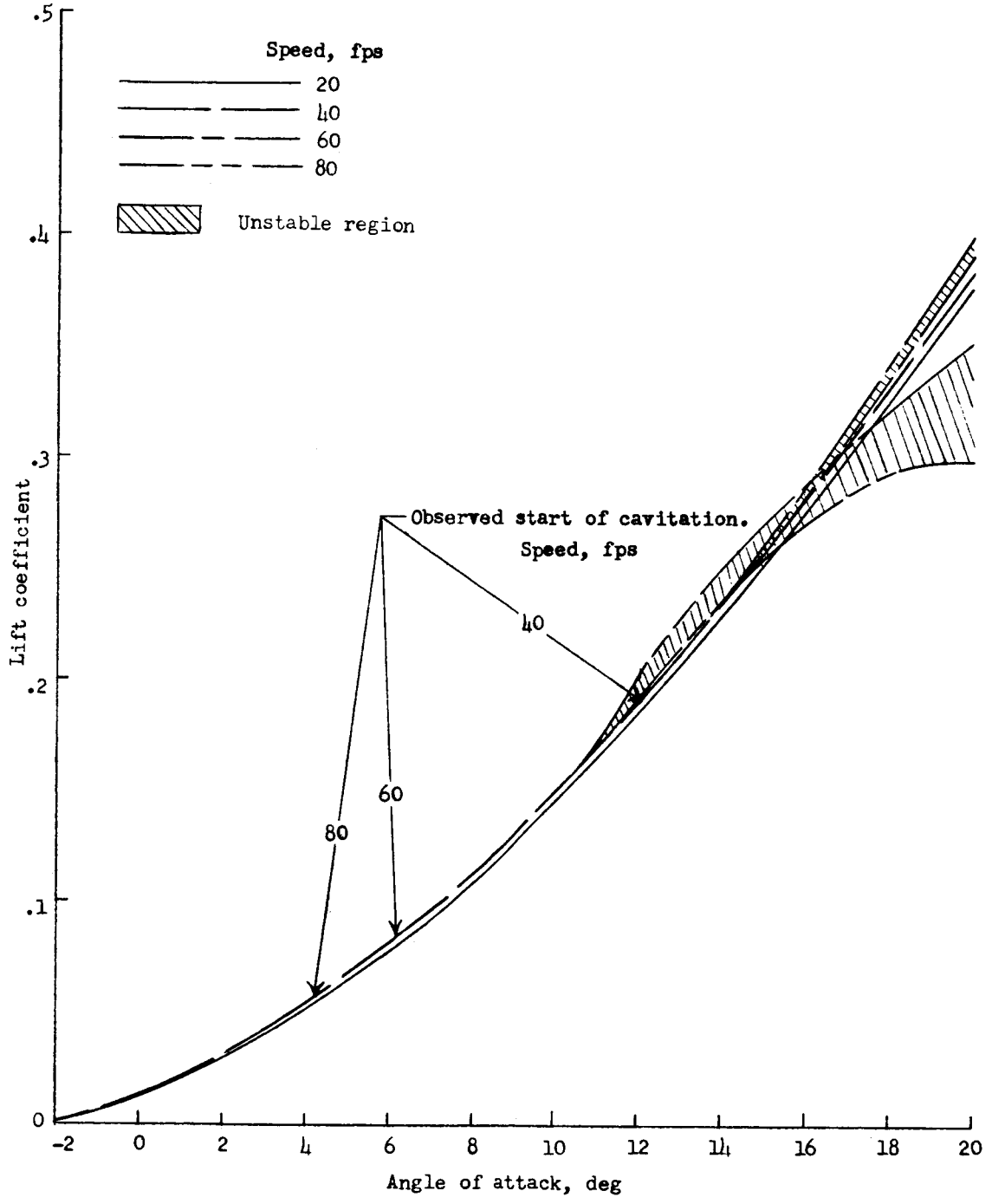

(b) Depth of submersion, 1.5 inches.

Figure 6.- Continued.

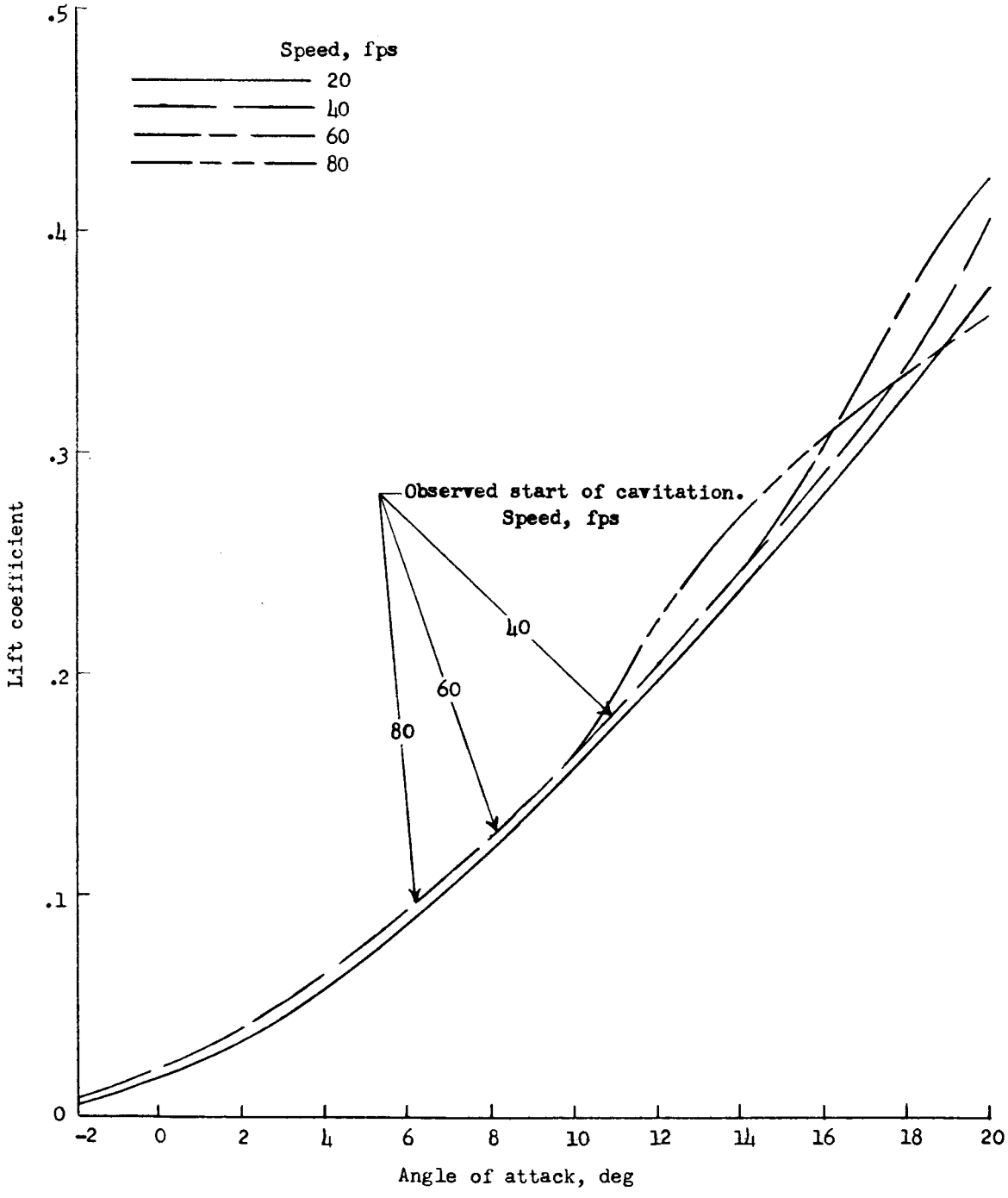

(c) Depth of submersion, 3.0 inches.

Figure 6.- Continued.

L-209

L-209

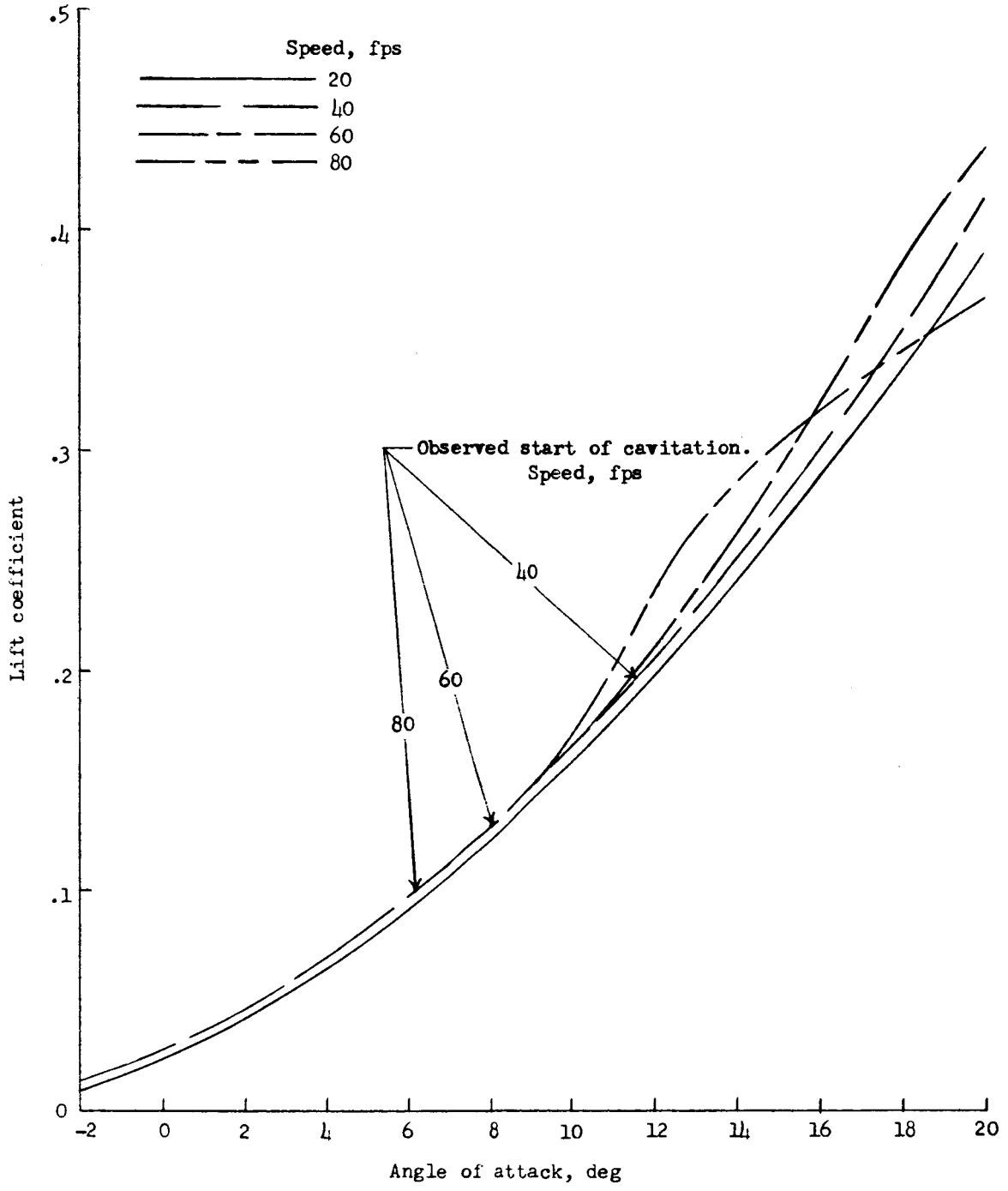

(d) Depth of submersion, 6.0 inches.

Figure 6.- Concluded.

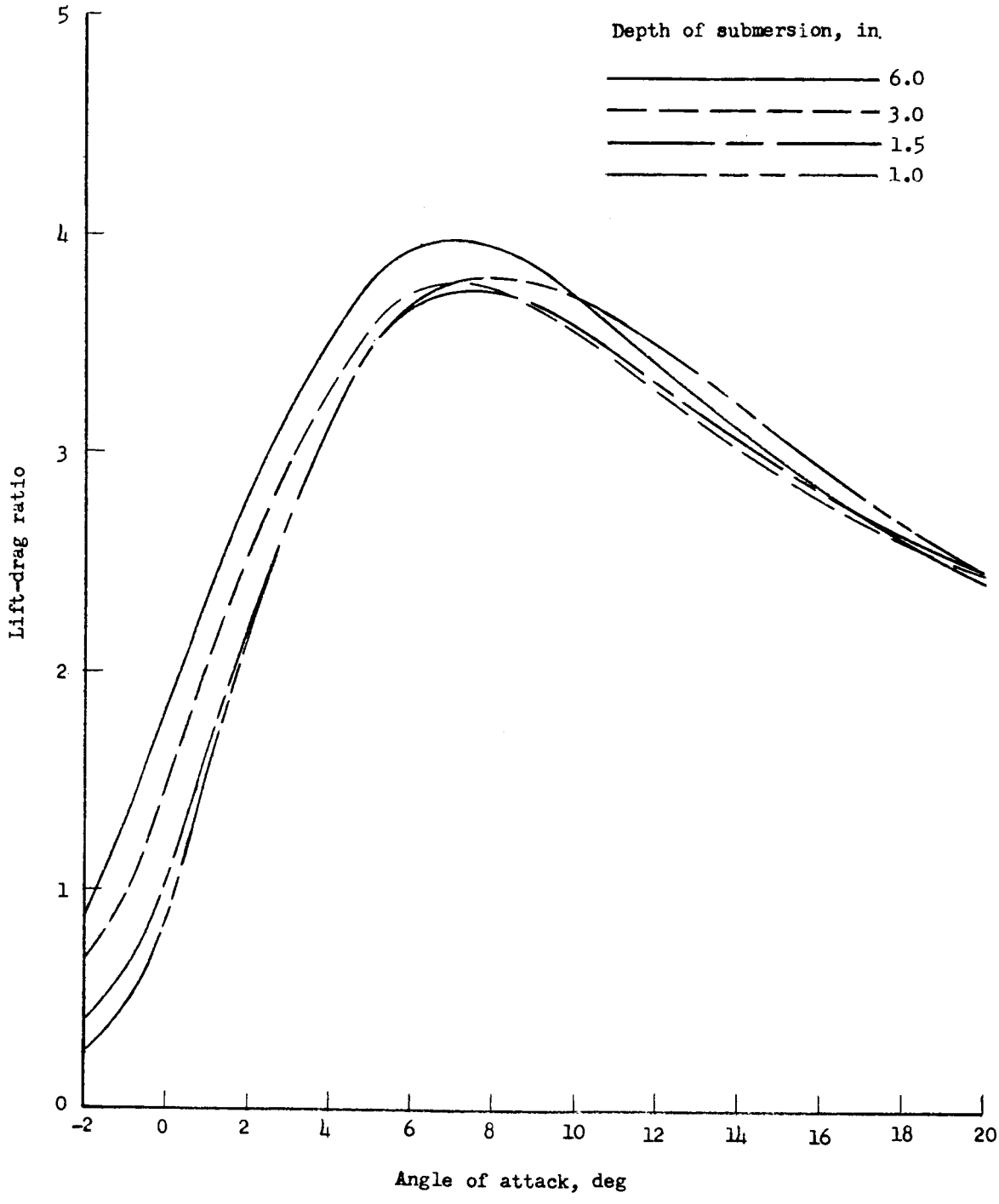

Figure 7.- Lift-drag ratio at a speed of 30 feet per second.

L-209

L-209

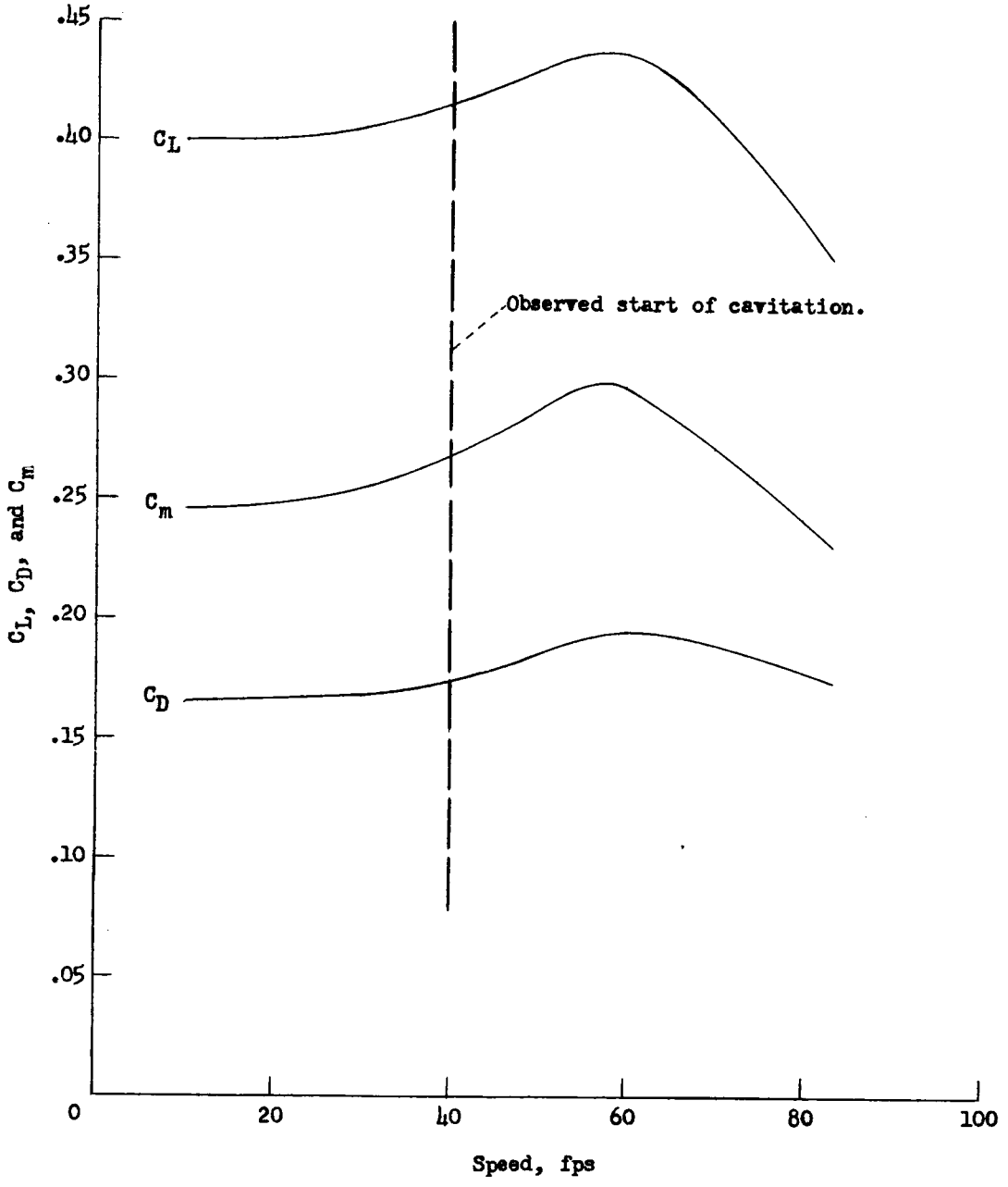

(a) Depth of submersion, 6.0 inches.

Figure 8.- Effect of cavitation on the force and moment characteristics at an angle of attack of 20°.

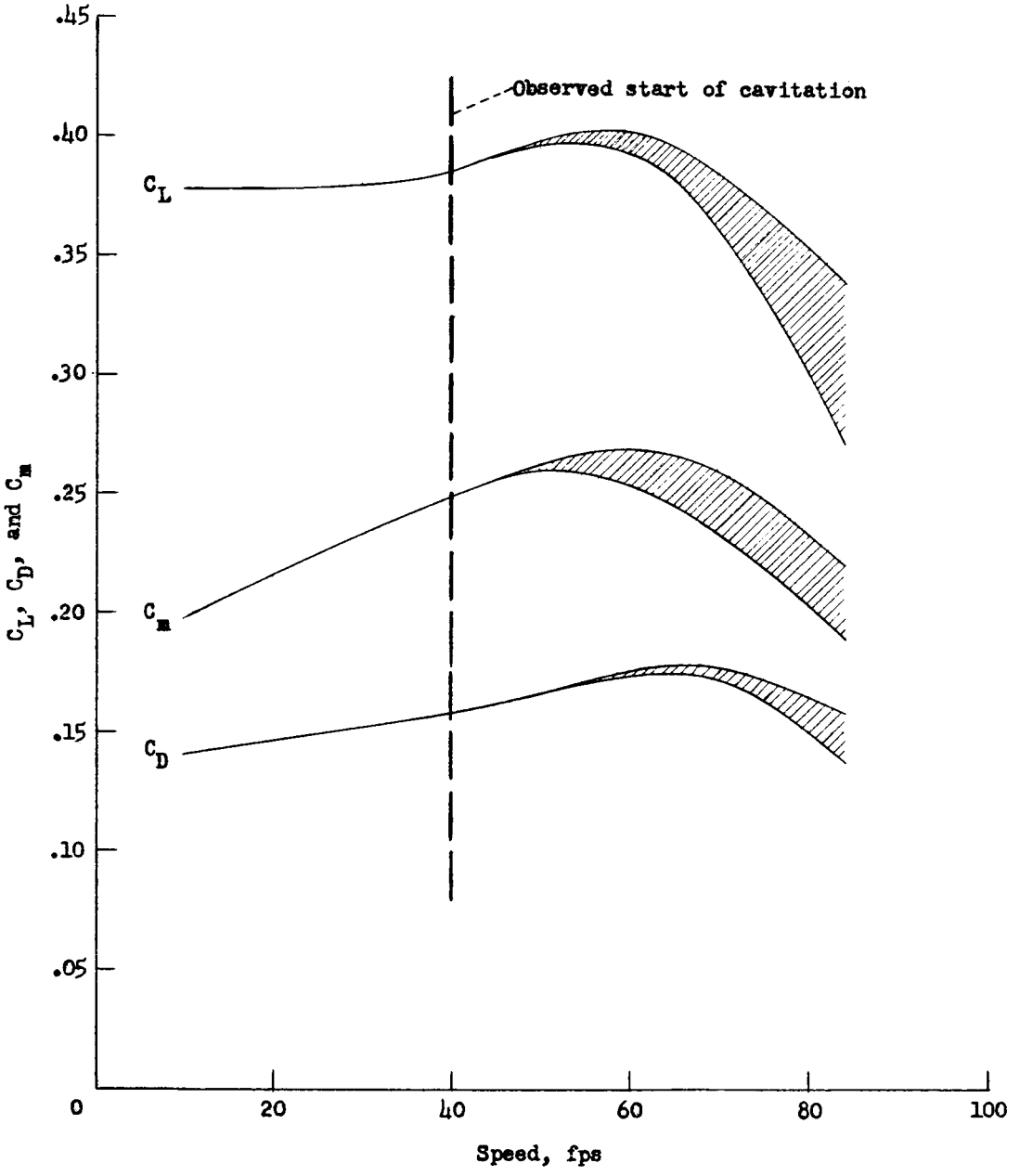

(b) Depth of submersion, 1.5 inches.

Figure 8.- Concluded.

L-209

L-209

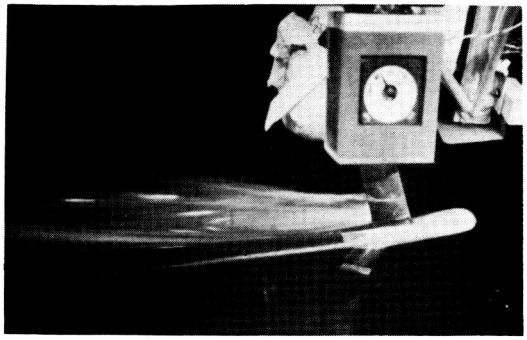

44.3 fps

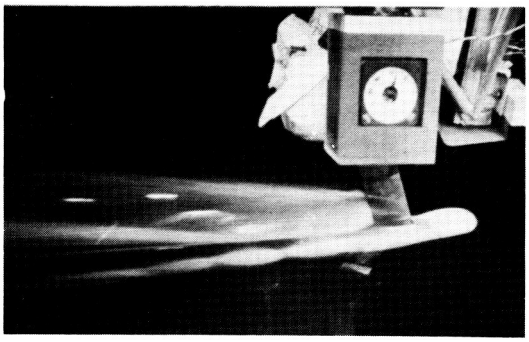

64.3 fps

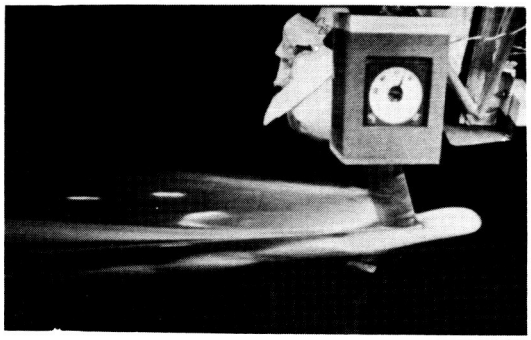

68.9 fps

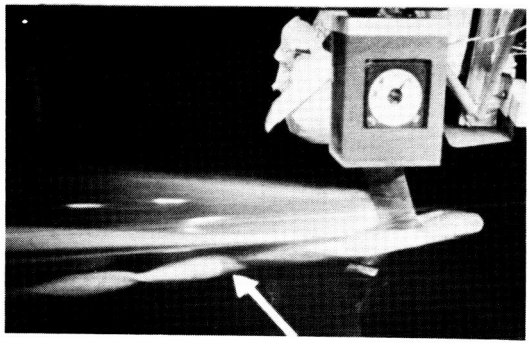

74.2 fps

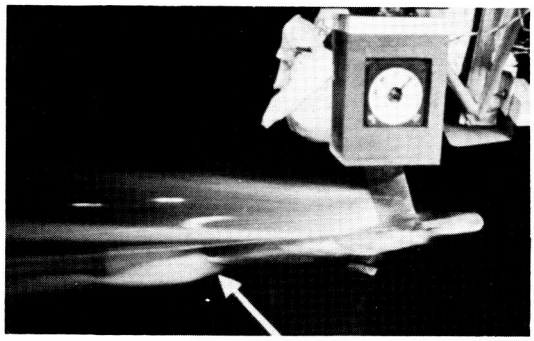

79.0 fps

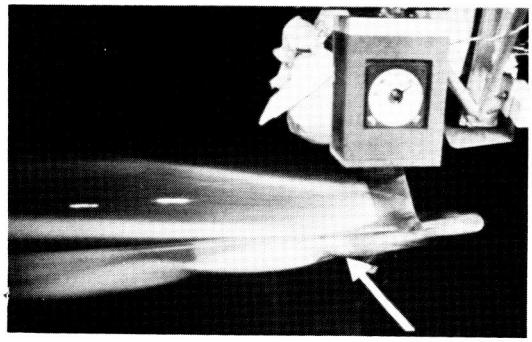

83.9 fps

L-59-3080

Figure 9.- Sequence photographs of a typical run showing the formation of cavitation at an angle of attack of 20° and a depth of submersion of 1.5 inches. The arrows indicate the most forward point to which air has been entrained in the trailing vortices.

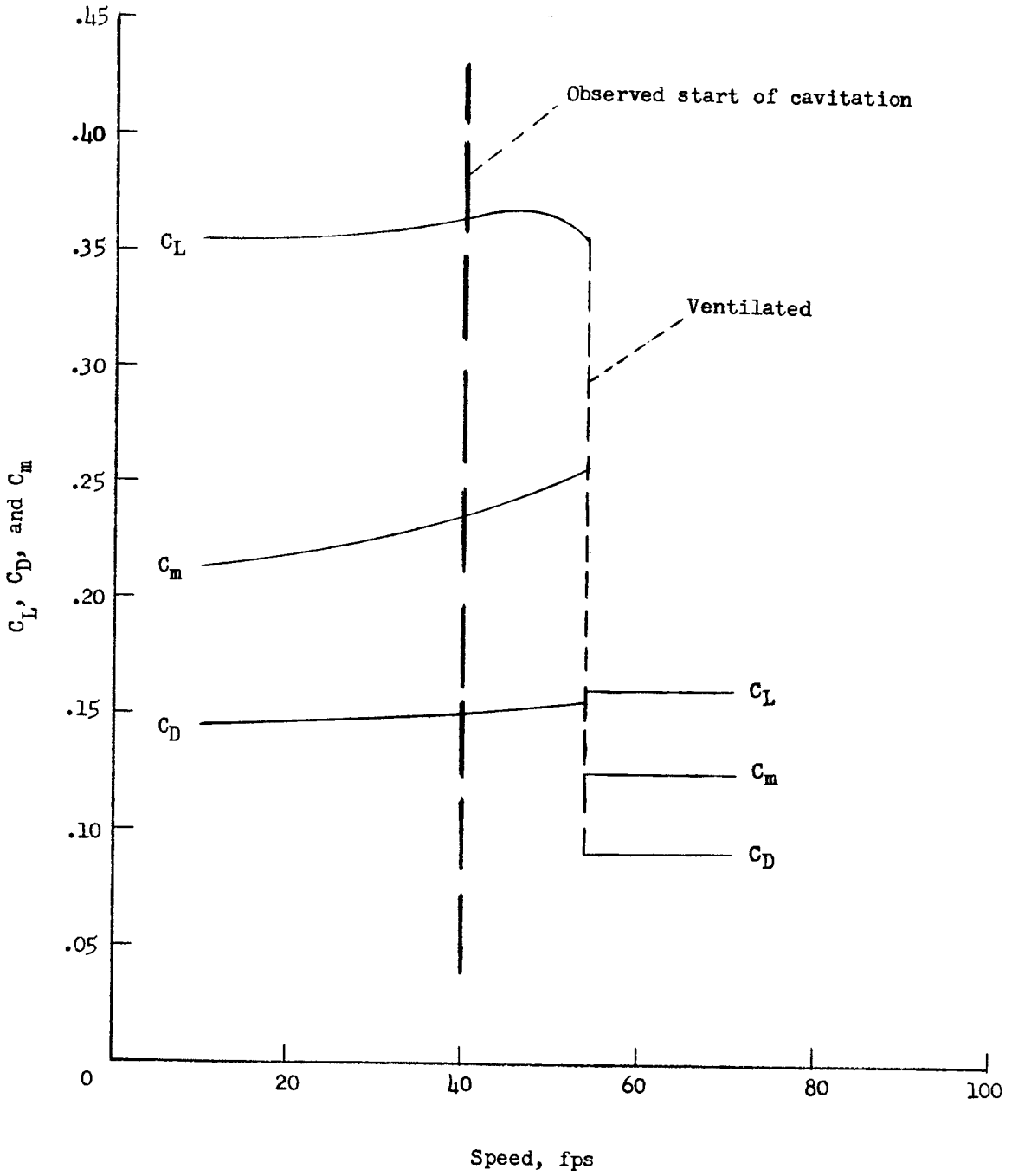

Figure 10.- Effect of ventilation (partial bubble) on the force and moment characteristics at an angle of attack of 20° and a depth of submersion of 1.0 inch.

L-209

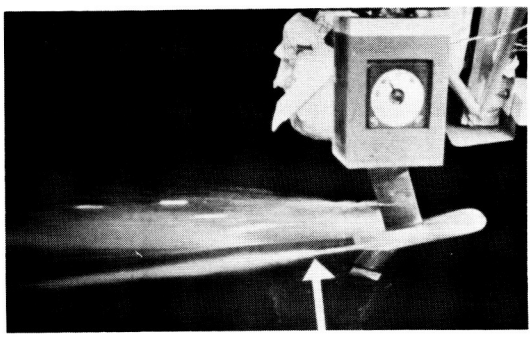

44.8 fps

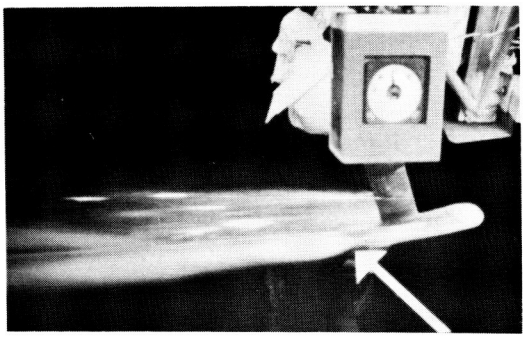

54 fps

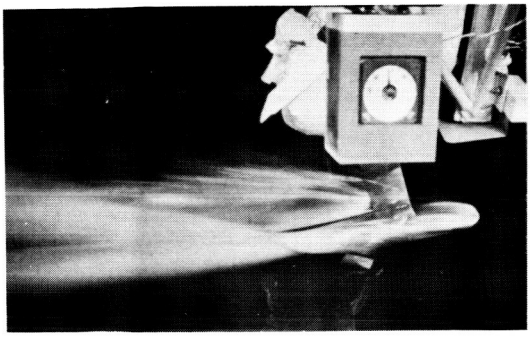

54 fps

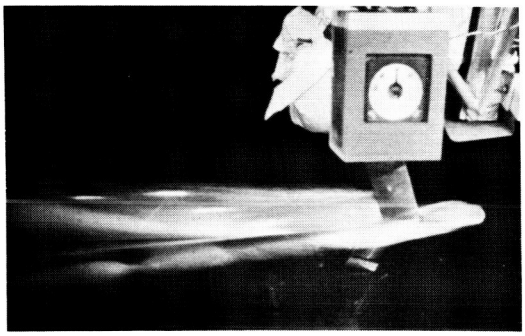

59.6 fps

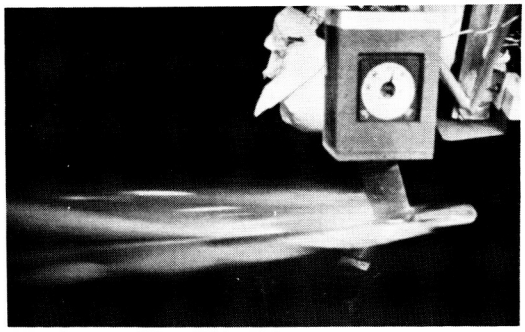

64.0 fps

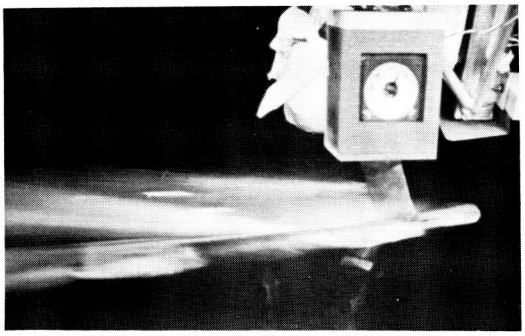

68.8 fps

L-59-3081

Figure 11.- Sequence photographs of a typical run showing cavitation and ventilation (partial bubble) with transition at a speed of 54 fps. The arrows indicate the most forward point to which air has been entrained in the trailing vortices. Angle of attack, 20°; depth of submersion, 1.0 inch.

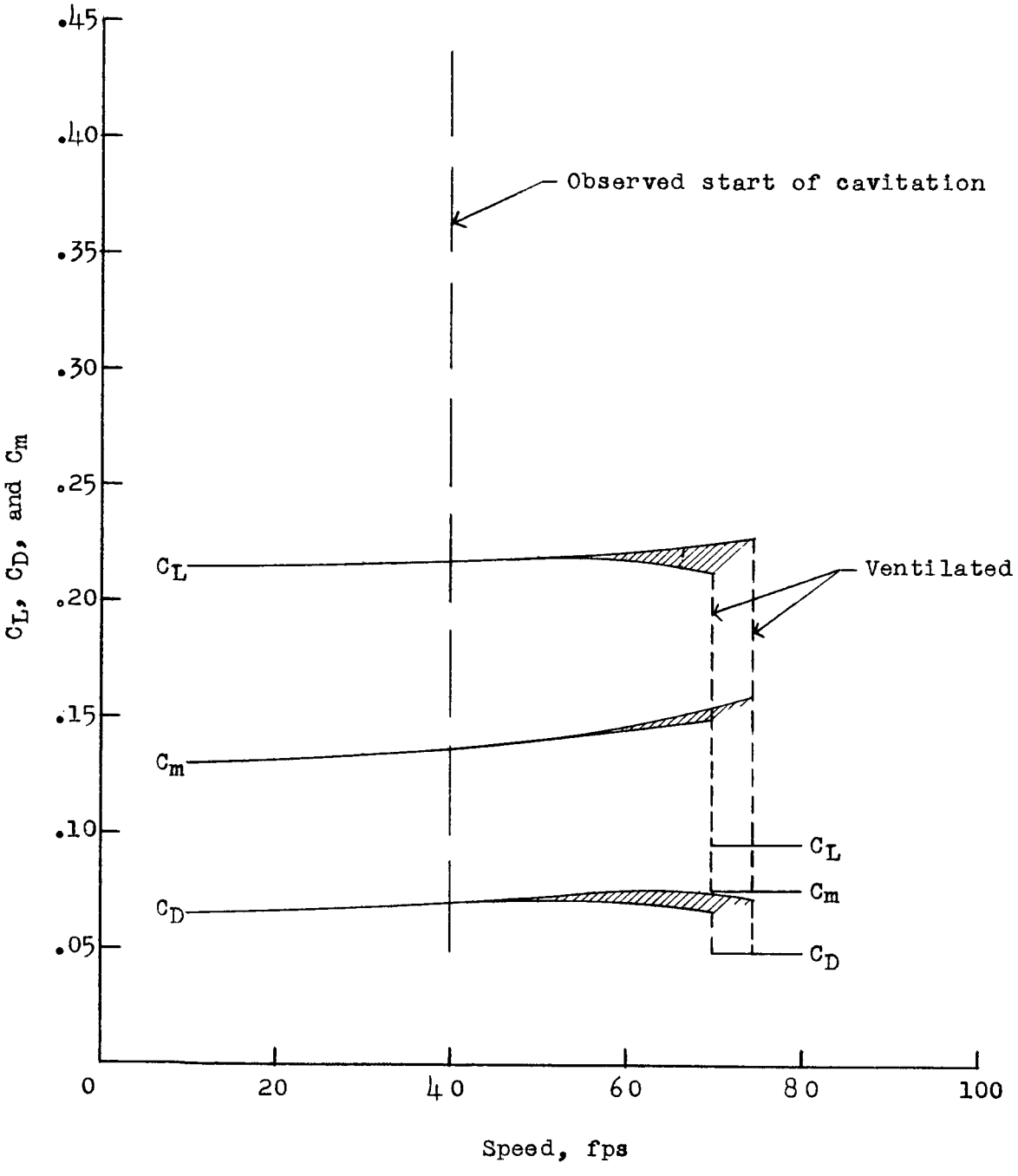

Figure 12.- Effect of ventilation (full bubble) on the force and moment characteristics at an angle of attack of 14° and a depth of submersion of 1.0 inch.

L-209

L-209

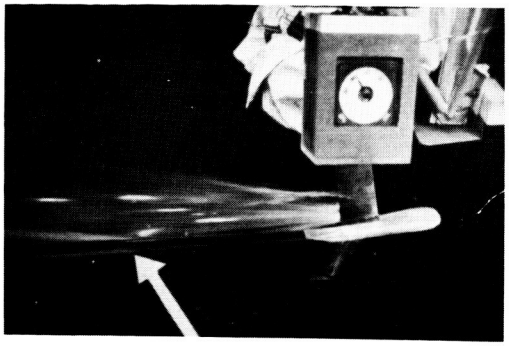

44.5 fps

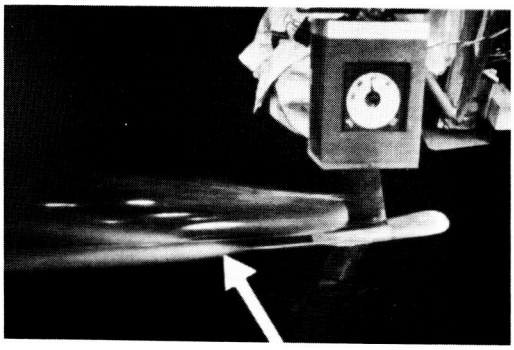

54.0 fps

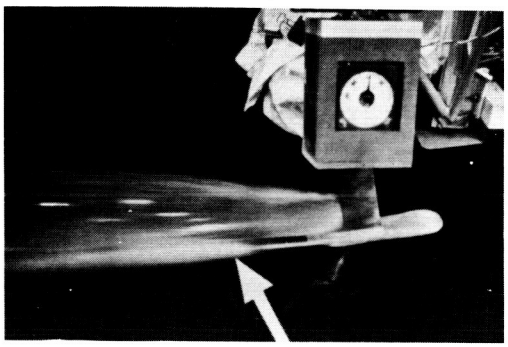

59.4 fps

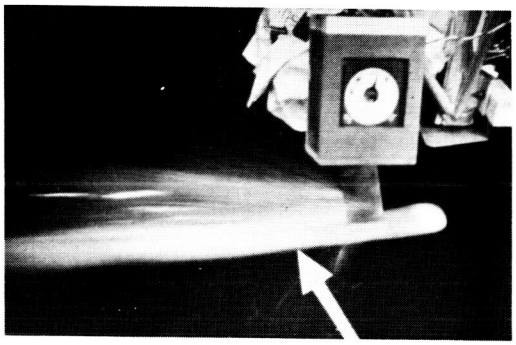

64.4 fps

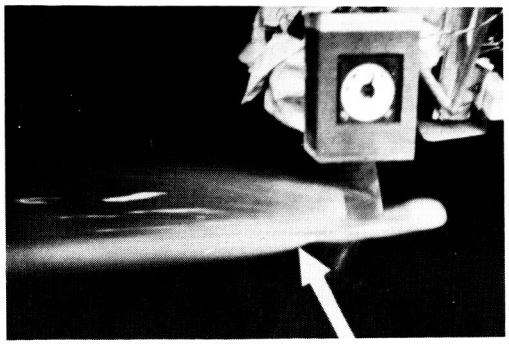

69.8 fps

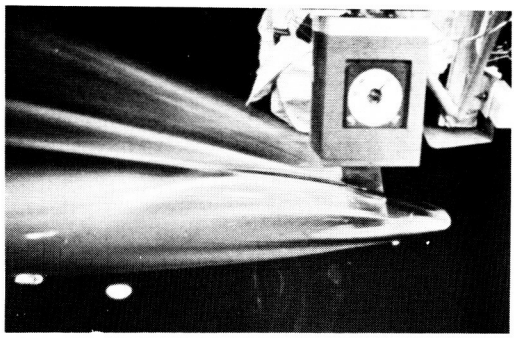

74.4 fps

L-59-3082

Figure 13.- Sequence photographs of a typical run showing cavitation, oscillation, and ventilation (full bubble). The arrows indicate the most forward point to which air has been entrained in the trailing vortices. Angle of attack, 14°; depth of submersion, 1.0 inch.

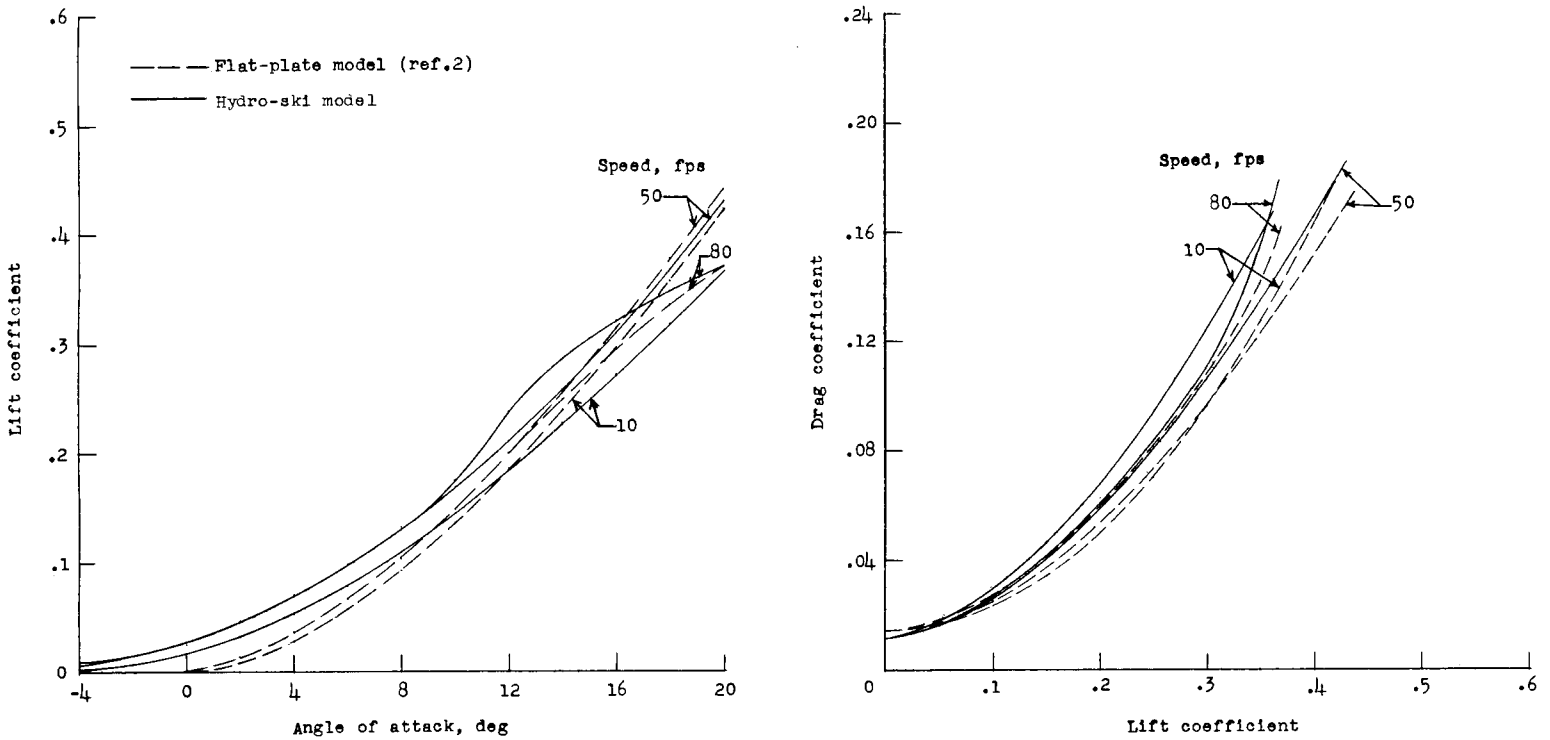

Figure 14.- Comparison of lift and drag characteristics at a depth of submersion of 6.0 inches.

L-209

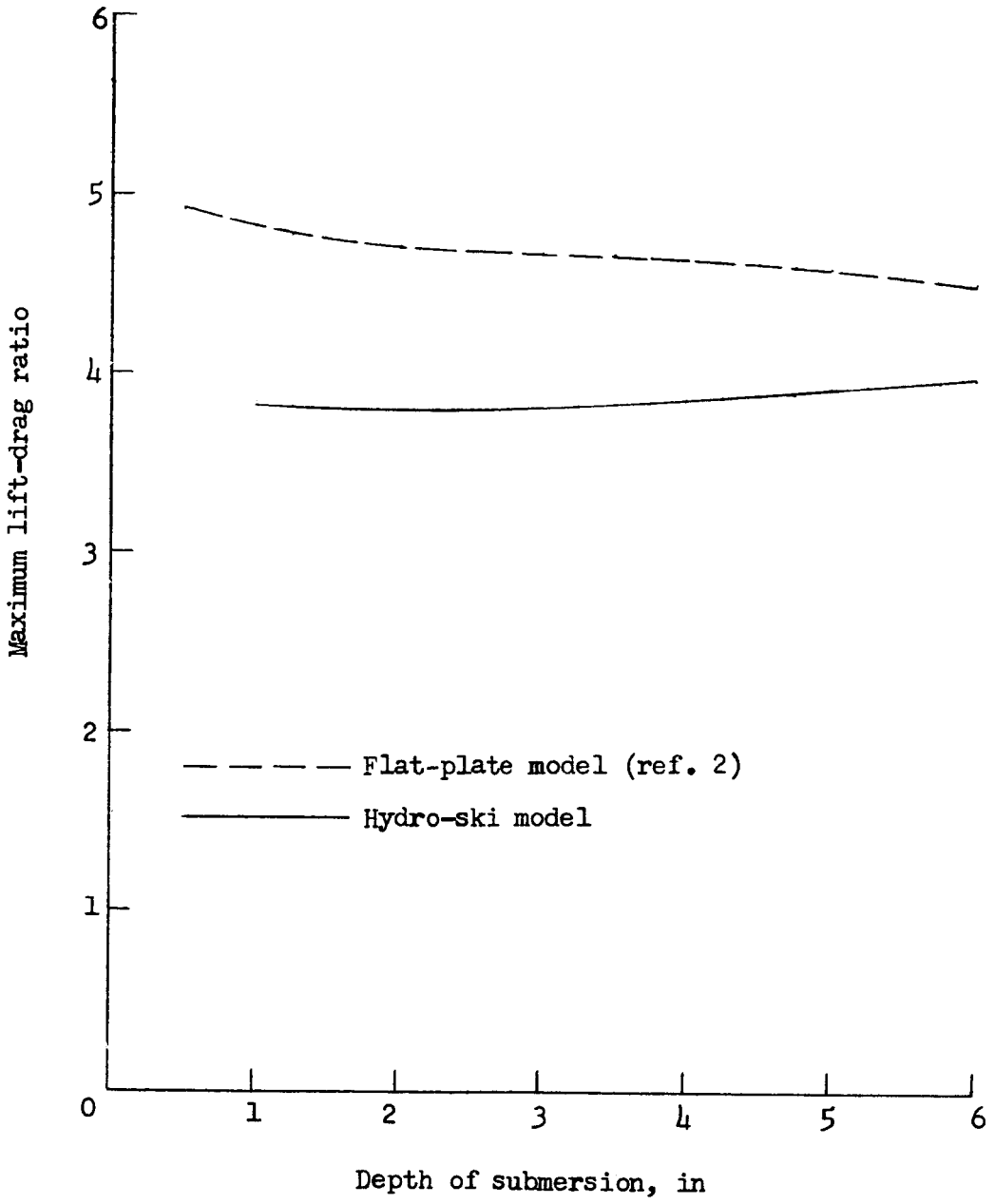

Figure 15.- Comparison of the maximum lift-drag ratio at a speed of 30 feet per second.

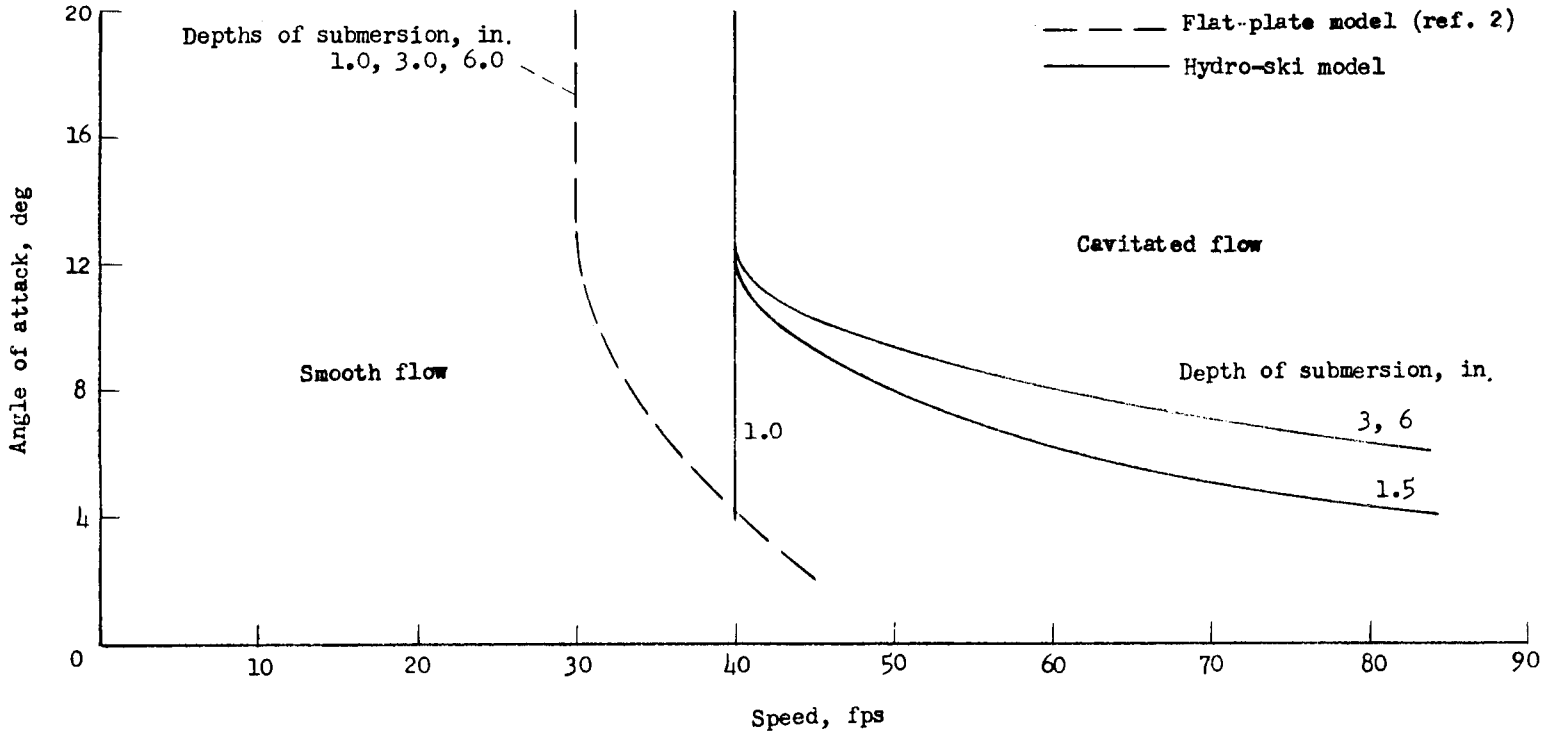

Figure 16.- Comparison of cavitation boundaries at various depths of submersion.

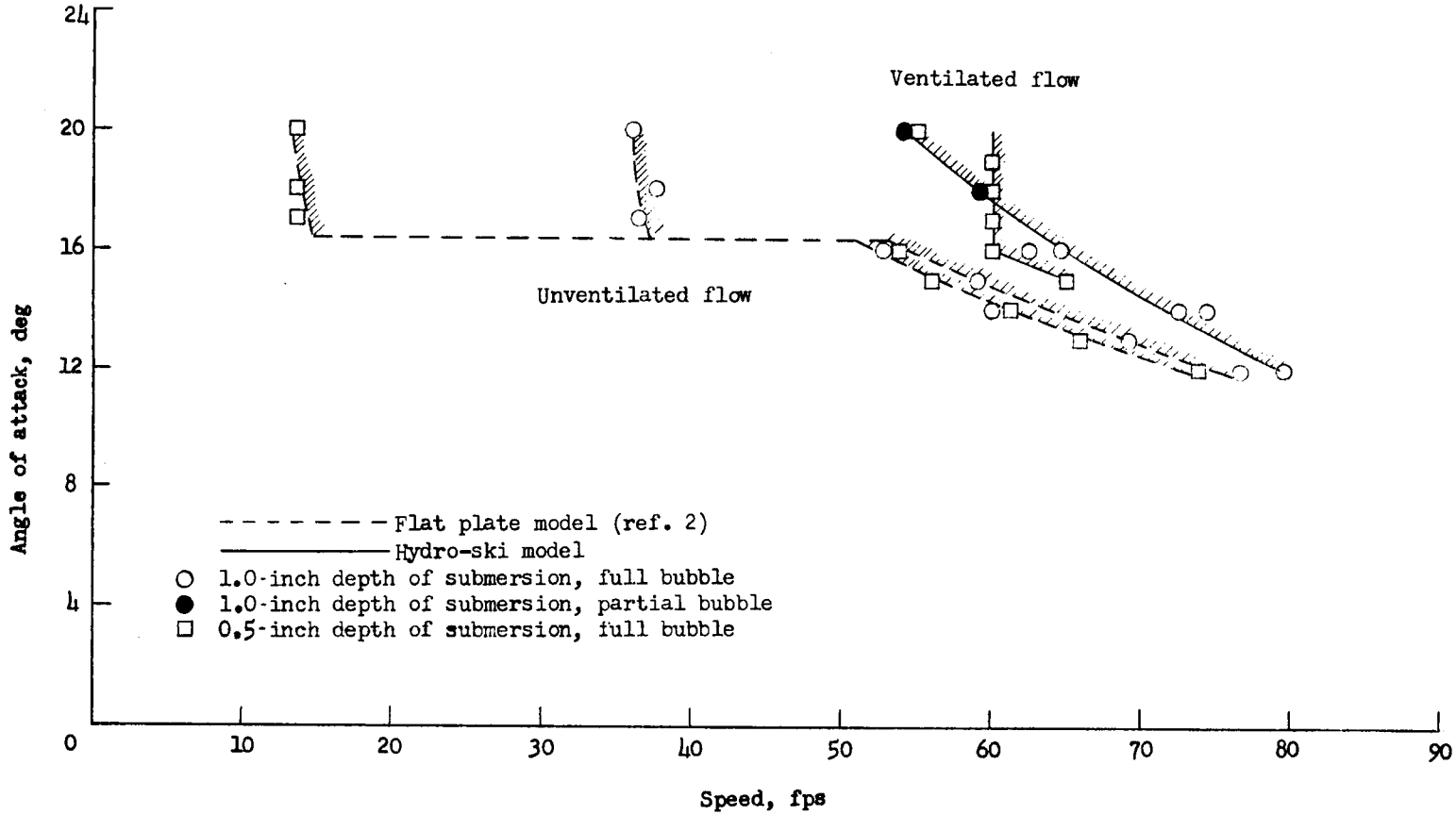

Figure 17.- Comparison of ventilation boundaries at depths of submersion of 1.0 inch and 0.5 inch.

NASA - Langley Field, Va. L-209